2012

Microstructure and mechanical properties of silicon carbide-titanium diboride ceramic composites

Derek Scott King

Department:

MICROSTRUCTURE AND MECHANICAL PROPERTIES OF SILICON CARBIDE-TITANIUM DIBORIDE CERAMIC COMPOSITES

by

DEREK SCOTT KING

A THESIS

Presented to the Faculty of the Graduate School of the

MISSOURI UNIVERSITY OF SCIENCE AND TECHNOLOGY

In Partial Fulfillment of the Requirements for the Degree

MASTER OF SCIENCE IN CERAMIC ENGINEERING

2012

Approved by

William G. Fahrenholtz, Advisor
Gregory E. Hilmas
David C. Van Aken

PUBLICATION THESIS OPTION

Sections in this thesis were prepared for publication in peer reviewed journals. Pages 1-27 contain an Introduction and a Literature Review for background purposes. Pages 28-56 were submitted as a paper to the Journal of the American Ceramic Society in June of 2012. Pages 57-84 will be submitted to Journal of the American Ceramic Society. Conclusions and Future Work sections are also included in pages 85-91. An Appendix is included for the purpose of presenting work that was performed, but not in either journal paper.

ABSTRACT

The microstructure, hardness, fracture toughness, Young's modulus, strength and Weibull modulus of silicon carbide-titanium diboride (SiC-TiB_2) ceramics were studied. First, SiC-TiB_2 ceramics with 15 vol.% TiB_2 particles were processed using two green processing methods, spray drying (ST) and ball milling (SiC-15TiB_2). In addition, SiC-TiB_2 ceramics with TiB_2 contents ranging from 0 to 100 vol.% were produced to determine a TiB_2 content that produced the best combination of mechanical properties. From spray drying, segregation of the TiB_2 particles in ST led to a granule-like microstructure and spontaneous microcracking in the final ceramic. In ceramics containing 20 and 40 vol.% TiB_2, the TiB_2 particle sizes were also large enough to allow for spontaneous microcracking. Spontaneous microcracking decreased the hardness from 28 GPa for SiC to 24 GPa for SiC-TiB_2 with TiB_2 contents of 80 vol.% or higher. In contrast, fracture toughness increased from 2 MPa·$m^{1/2}$ for SiC to ~6 MPa·$m^{1/2}$ for SiC containing 40 vol.% TiB_2 or more. Using a two-parameter Weibull analysis, SiC with 20 vol.% TiB_2 had the highest average strength (522 MPa), followed by SiC-15TiB_2 (500 MPa), then SiC with 40 vol.% TiB_2 (420 MPa), and ST (380 MPa). While microcracking in ST lowered the strength, hardness, and elastic modulus compared to SiC-15TiB_2, the granule-like microstructure combined with microcracking, narrowed the flaw size distribution of ST and boosted the Weibull modulus of ST to 21 compared to 12 for SiC-15TiB_2, which had a uniform distribution of TiB_2 particles. The Weibull moduli of SiC containing 20 and 40 vol.% TiB_2 was also boosted to 17, compared to 12 for a TiB_2 content of 15 vol.%. To maximize each property, TiB_2 particle sizes should be kept just below the spontaneous microcracking threshold to prevent spontaneous flaw formation.

ACKNOWLEDGEMENTS

I would first like to thank my advisors Drs. William Fahrenholtz and Gregory Hilmas for guiding and supporting me throughout my time as a Masters student. Throughout my time they have allowed me to present my work through conferences and publications. Dr. Fahrenholtz especially has given me many pointers on the finer aspects of technical writing which I greatly appreciate. I would also like to thank them for extending the opportunity for me to stay at Missouri S&T to continue my graduate work. I would also like to thank my final committee member, Dr. David Van Aken, for his time.

I would like to acknowledge that work for my Masters was funded by Saint-Gobain Advanced Ceramics and the Army Research Laboratory through Cooperative Agreement Number W911NF-08-2-0001. Drs. Fahrenholtz and Hilmas also deserve more credit for nominating me for the Chancellors Fellowship which has assisted in financing my tuition and fees.

Next, I would like to extend gratitude to my laboratory colleagues in 307 McNutt. Their use of prior experience, circular reasoning, and subject dodging has "helped" me throughout my graduate studies. All joking aside, thank you to Dr. Jeremy Watts, Dr. Harlan Brown-Shaklee, Dr. Matt Thompson, Greg Harrington, Eric Neuman, Ben Lai, Maryam Kazemzadeh Dehdashti, and Jason Lonergan.

Lastly, I would not be here without the love and support of my family. To my mother and grandmother, I cannot begin to understand the sacrifices the two of you have made as I have grown and I truly appreciate everything. To my fiancé, Liz Stahlman, you have supported me every step of the way and I am forever grateful.

TABLE OF CONTENTS

Page

PAPER

SECTION

LIST OF ILLUSTRATIONS

PAPER II

LIST OF TABLES

1. INTRODUCTION

The research described in this thesis examines the microstructure and mechanical properties of silicon carbide-titanium diboride ceramic composites, which are candidates for use as ceramic armor. A commercial powder consisting of silicon carbide containing 15 vol.% titanium diboride particles (Hexoloy ST, St. Gobain Advanced Ceramics, Niagra Falls, NY) was the baseline composition for comparison to ceramics produced by mixing SiC and TiB_2 powders. In order to maximize the properties of the ceramic for armor, SiC-TiB_2 composites ranging from nominally pure SiC to nominally pure TiB_2 were also produced for characterization across the composition range.

The concept of body armor has existed as long as humans have desired protection from the outside environment.[1] The simplest form of body armor has existed since humans have been able to manufacture clothing. The word armor is now generally associated with a material that protects a soldier in combat. Similarly, early armor examples stem from our images of Spartan and Roman soldiers who used metal helmets and breast plates as well as thick leathers.[2,3] In later times, knights wore full suits of steel armor with chain mail underneath.[3] More recently, advances in the processing of polymers, metals, and ceramics have led to advances in armor. Modern day body armors range from textiles such as Kevlar® that offer protection from small firearms to advanced ceramics such as SiC that offer protection from armor piercing rounds.[4]

In modern body armors, ceramics such as SiC and B_4C have advantages over metals and other materials due to their low densities and high hardness. B_4C has one of the lowest density values of structural ceramics at 2.52 g/cm^3.[5] In contrast, iron, which is used for steel-based armors, has a density of 7.87 g/cm^3, which is more than three times

that of B_4C.[6] While any armor may be bulky and stiff, the weight reduction that comes with the use of ceramic armor is an advantage for a soldier on the move in any conditions.

Because of their high hardness, advanced ceramics are also used in applications where armor piercing rounds are a threat. The high hardness exhibited by some ceramics allows for an increase in the dwell time of a projectile on the surface of the ceramic, which aids in the erosion and defeat of the projectile.[6,7] The hardness of ceramics such as SiC (20-27 GPa), B_4C (22-37 GPa), and TiB_2 (25-35 GPa) meet this high hardness requirement.[6-12]

Ballistic impact is a very complicated process, which makes it difficult to use one mechanical property as a factor to predict projectile defeat. Because of this, most ceramic armors are selected by testing them in their desired application for a "pass or fail" grade. While hardness has been identified as one factor that can be used to predict projectile defeat, fracture toughness and strength are factors that relate to multi-hit capabilities.[6] Fracture toughness, in particular, is an area where SiC ceramics have room for improvement. Reported values for fracture toughness of SiC range from 2 to 9 $MPa \cdot m^{1/2}$. However, an increase in fracture toughness is typically accompanied by a decrease in hardness.[13,14] Reported fracture toughness values for SiC ceramics with hardness >20 GPa typically fall in the range of 2.5 to 4 $MPa \cdot m^{1/2}$.[7,8] To combat the drop in hardness that is typically seen with an increase in fracture toughness, TiB_2 particles can be added to SiC as a reinforcing phase. SiC-TiB_2 ceramics have shown the ability to retain a high hardness while also showing improved toughness. For example, SiC-TiB_2

ceramics with hardness , >23 GPa and toughness >4 MPa·$m^{1/2}$ have been reported, which are an improvement compared to nominally pure SiC ceramics.[15,16]

Previous studies on SiC-TiB_2 composites have tended to focus on maximizing one mechanical property, such as hardness or fracture toughness. In contrast, the research reported in this thesis examines green processing effects, hardness, fracture toughness, and Weibull modulus. Some of the technical questions addressed by this research include:

1. What affect does green processing, spray drying compared to mechanical mixing, have on the final ceramic composite?
2. How do TiB_2 additions affect the microstructure and mechanical properties of the SiC matrix?
3. Does a specific composition exhibit a superior combination of hardness, fracture toughness, and Weibull modulus?

To answer these questions, mechanical properties including Vickers hardness, fracture toughness, and Young's modulus were measured as a function of TiB_2 content for SiC-TiB_2 ceramics. Using a two-parameter Weibull analysis, the strengths were compared for different TiB_2 contents. Microstructural analysis was also completed using optical and scanning electron microscopy techniques.

2. LITERATURE REVIEW

2.1 CERAMIC ARMOR

Interest in ceramic armor grew in the 1960's during the Vietnam War as a way to protect night watch guards from snipers.[17] Metal/fiber composites like aluminum backed with fiberglass became popular as the first ceramic-containing systems tested ballistically, but they performed poorly.[17] Weight quickly became an issue for ground crews, a factor that became a bigger issue when trying to protect air crews in the Huey helicopters used during Vietnam.[18] After initial testing and resulting design changes, ceramic armors became highly desired for their light weight and high hardness.[6,7,10,11,19] In the late 1980's, Hauver discovered that as hardness increased, so did the dwell time of a projectile.[7,10,17,20] Increased dwell time led to increased erosion of the projectile which aided in defeat of the projectile.[20] Silicon carbide (SiC), aluminum oxide (Al_2O_3), boron carbide (B_4C), and titanium diboride (TiB_2) are some ceramics in this class of light weight/high hardness materials that are used for armor applications.[6,8,18,20,21] Densities for these materials ranges from 2.52 g/cm^3 for B_4C to 4.52 g/cm^3 for TiB_2.[5,9] Table 1.1 lists the hardness of these ceramics along with the hardness of some commercial armors.

Table 1.1. Ceramic Materials used in Armor Applications

Material	Density (g/cm^3)	Hardness (GPa)
SiC[8,12,18]	3.20	20-27
Al_2O_3[12,18]	3.98	11-17
B_4C[5]	2.52	22-37
TiB_2[9,12]	4.52	25-35
SiC-B (Cercom)[8]	3.21	20.6±1.2
SC-RB (Coors Tek)	3.10	24.5
SiC-N[22]	3.20	27.2±1.8
SiC-SC-1RN[22]	3.20	28.9±1.9
CAP 3 (Coors Tek)	3.90	14.1

While high hardness is an essential property for armor ceramics because of its relation to projectile damage, no one mechanical property can be used to predict the behavior of armor systems. Young's modulus affects the propagation of stress waves through the ceramics, strength and fracture toughness control multi hit capability, and fracture mode can act as another energy absorber.[6] In addition, microstructural characteristics can also have a major effect on the mechanical properties, which, in turn, affect ballistic performance. Microstructural characteristics such as grain size, second phases, and porosity affect each of the aforementioned mechanical properties.[6,23-28] Typically an increased toughness can be achieved with an increase in grain size; however, hardness typically decreases when toughness increases, which is an example of

the classic hardness/toughness tradeoff that has been reported for other materials.[7,8] Large pores can act as strength limiting flaws while increasing amounts of porosity can also drastically reduce the Young's modulus and hardness, which makes a dense ceramic better for armor.[29] Section 2.3 further discusses the effects of microstructure on the mechanical properties, but it is important to understand that microstructures can be controlled to maximize specific properties.

The brittle nature of ceramics and the resulting low fracture toughness raise concerns about fragmentation and multi hit capability of ceramics in armor applications. Because of these concerns, composite armor systems often use a ceramic front that is laminated to a metal or woven fabric backing to help control fragmentation and absorb energy during defeat of a projectile.[18,30] Still, just as one property cannot be used to predict the performance of an armor system, one armor system is not ideal for every application. Textiles such as Kevlar® are typically used for low level threats such as the National Institute of Justice (NIJ) level III or lower where a level III armor must be able to stop a rifle fired, steel jacketed bullet of 9.6 g at a velocity of 850 m/s. However, hard ceramic armors are needed in some cases for NIJ level III and higher where armor piercing rounds may be used.[4] Armor piercing rounds being .30 caliber with a mass of 10.8g, fired at a velocity of 878 m/s as specified by the NIJ standard.[4]

2.2 MECHANICAL PROPERTIES

2.2.1 Hardness. Materials can deform elastically and plastically. In linear elastic materials, such as ceramics, elastic deformation occurs when a stress is applied and the material reacts by deforming. When the stress is removed, the material will recover its

original shape. Plastic deformation occurs when a large enough load is applied to move outside of the linear elastic region and the material cannot recover to its original shape. Because of the way it is typically measured, hardness can be considered the resistance of a material to non-recoverable plastic deformation.[29,31]

Hardness is measured by indenting the surface of a material with a sharp tip. The magnitude of hardness is typically calculated using Equation 2.1 where H is the hardness, P is the indention load, and "a" is the projected dimension of a Vickers indent. Figure 2.1 of a Vickers indent shows an example of the contact area of an indentation. The units of hardness are load per unit area, which gives units of pressure. Therefore, an alternative definition of hardness is the pressure required to produce a certain amount of non-recoverable plastic flow.[32]

$$H = \frac{P}{2a^2} \tag{2.1}$$

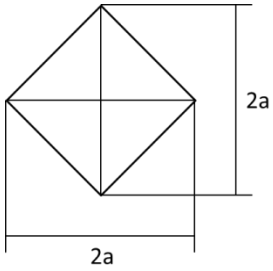

Figure 2.1. Schematic diagram of a Vickers indent showing the contact area of the indent and the "a" dimensions.

Hardness can be used for quality control measures and its value affects wear, erosion, and machining damage.[33] For ceramics, hardness is typically measured using

one of two methods, Vickers or Knoop indentation.[29] The Vickers hardness of a ceramic is determined by indenting with a pyramid shaped indenter (Figure 2.1) and the diagonal dimensions of the resulting indent are measured to determine the contact area.[29] However, a Knoop indenter tip has a length to width ratio of 7:1, which spreads the load out over a much larger area. This not only changes the deformation zone under the indenter tip, but also reduces the amount of cracking compared to Vickers indents.[29,34] When measuring a Knoop indent, only the length of the long axis is measured. Based on the geometry of the indent, the projected area of the indent is calculated rather than the contact area. Hardness also changes with the load used to produce the indent, a phenomenon that is known as indention size effect (ISE). Hardness values reach a plateau when the load is large enough which can be determined by measuring hardness with several different loads. Therefore, to fully characterize the hardness of a ceramic, it is important to understand ISE so measured hardness is a measure of the upper limit of non-recoverable deformation of a ceramic.[26,29,34]

2.2.2 Young's Modulus. The Young's modulus, also known as the elastic modulus, is representative of the energy required to produce elastic deformation between bonds in a material.[35] The Young's modulus, can mathematically be defined as the change in stress (σ) (load per unit area) as a function of the change in strain (ε) (change in length per unit length) as defined by Hooke's law and shown in Equation 2.2 where E is the Young's modulus.[29]

$$\varepsilon = \frac{\sigma}{E} \tag{2.2}$$

In practice, the Young's modulus of a material is typically measured using either static or dynamic measuring techniques. The simplest of static techniques is tensile testing where the stress and strain can be recorded during strength testing. Stress as a function of strain curves can then be plotted. For linear elastic materials such as ceramics the slope of the stress-strain curve is the Young's modulus.[36] Flexure testing is more common due to simple sample geometry, however, Young's modulus measurement errors can occur due to non-uniform stress distribution as well as plastic deformation during flexure testing.[29]

Dynamic techniques can be more accurate for determining Young's with measurement error of less than 0.1%.[37] In these methods, modulus is determined by detecting resonant vibrations or ultrasonic wave propagation through the material.[29] Using impulse excitation as described in ASTM C1259-08^{E1}, a flexure wave is sent through a rectangular bar of length L, width w, thickness t, and mass m.[37] The frequency of the flexure wave (f_f) can be detected using a piezoelectric transducer and then used in Equation 2.3 to determine Young's modulus (E) where T_1 is a correction factor defined in the standard. Compared to static testing methods, the measurement of Young's modulus through dynamic testing methods does not require the destruction of samples. Using the same sample, torsional waves can be set up in the material and their frequency can be also be measured. This allows for the measurement of shear modulus and Poisson's ratio.[37]

$$E = 0.9465\left(\frac{mf_f^2}{w}\right)\left(\frac{L^3}{t^3}\right)T_1 \qquad (2.3)$$

2.2.3 Strength. The strength of a material is a relative measure of the stress required to break bonds in that material and can, therefore, be defined as the maximum stress that a material can withstand at fracture.[29] With its roots buried in atomic bonding, strength is derived from the Coulombic attraction and a repulsive force from electron orbitals acting on them.[29,35,38] Shown in Figure 2.2, atoms in a lattice have a preferred separation distance based on a balance between the attractive and repulsive forces. If an external force (P) is applied, the atoms will move relative to each other, changing their equilibrium position. However, to break a bond, a force greater than the cohesive force (P_c) must be applied to the atomic lattice. By idealizing the force-displacement relationship as a sine wave, the cohesive force can be defined with Equation 2.4 where λ is the change in atomic spacing when a bond is deformed, and x is the displacement. The bond stiffness, k, can be determined using Equation 2.5 where k is the load/displacement ratio. Dividing Equation 2.5 by the number of bonds per unit area, the force required to break atomic bonds becomes the cohesive stress (σ_c) and the bond stiffness becomes the Young's modulus. Using this approach, Equation 2.5 can be re-written as Equation 2.6 which is the base equation for the theoretical strength of a material.[35]

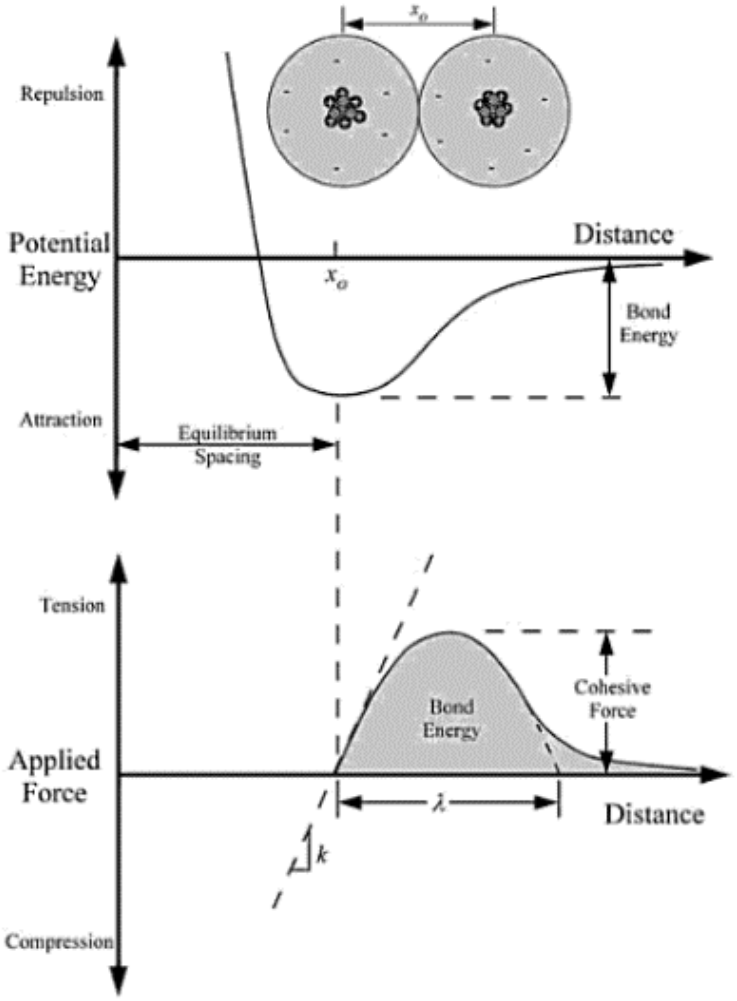

Figure 2.2. Potential energy as a function of atomic spacing where x represents the equilibrium spacing between atomic nuclei.[35]

$$P = P_c \sin(\frac{\pi x}{\lambda}) \tag{2.4}$$

$$k = P_c \left(\frac{\pi}{\lambda}\right) \tag{2.5}$$

$$\sigma_c \approx \frac{E}{\pi} \tag{2.6}$$

For brittle materials, the theoretical strength over-estimates the actual strength because of stress concentrators such as weak bonding between grains or flaws such as pores and microcracks within the bulk material. Ultimately, stress concentrators reduce the maximum attainable strength.[29] Griffith used the first law of thermodynamics to model the effect of flaws on strength. Assuming that a crack propagated fast enough that heat flow was negated, Griffith's proposed that the mechanical work put into the sample was equal to the sum of elastically stored potential energy and the surface energy at a crack tip.[29,39] Using Equation 2.7, Griffith showed for plane stress conditions that the fracture of a brittle solid under stress (σ_f) was controlled by a critical flaw size ($2c_c$), but was also related to the Young's modulus and the surface energy per unit area of a crack (γ).[29] It was later shown that the thermodynamic value of γ should actually be replaced by the larger value of fracture surface energy (γ_f).[29]

$$\sigma_f = \left(\frac{2E\gamma}{\pi c_c}\right)^{\frac{1}{2}} \tag{2.7}$$

To measure the strength of brittle materials, flexure testing is typically used due to its low cost and simple specimen geometry.[29,40] ASTM C1161-02c describes the guidelines for testing the strength of brittle solids in flexure. Both three and four-point flexure testing are popular methods for measuring flexure strength. The strength can be determined by measuring the load required for failure and calculating strength with Equation 2.8 where M is the bending moment, y is the distance from the neutral axis, and I is the moment of inertia.[41] Shear and moment diagrams are shown in Figure 2.3 for three-point and four-point flexure tests. From the shear diagrams, it can be seen that

shear is present across the entire bar during three-point bending. It can also be seen that the moment is not constant across the bar. Conversely for four point flexure, the shear force is neutralized and the bending moment is constant between the top loading pins. This makes four-point flexure a true measure of the strength in bending since three point bending is influenced by shear forces. Still, tensile testing provides the truest measure of strength.[29]

$$\sigma = \frac{My}{I} \tag{2.8}$$

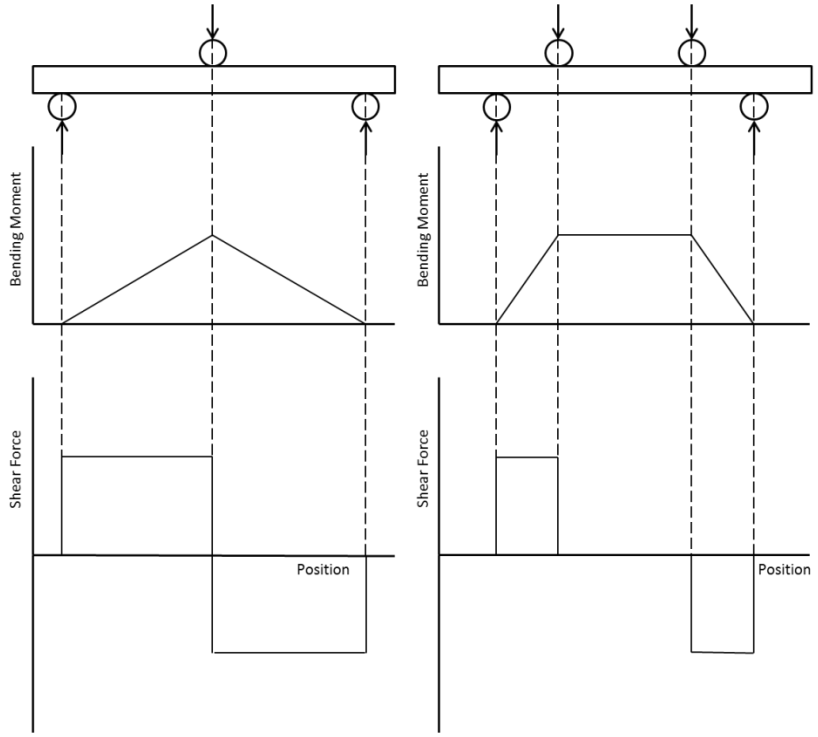

Figure 2.3. Shear and moment diagrams for three-point (left) and four-point (right) flexure testing techniques.

2.2.4 Fracture Toughness. While strength is controlled by the presence of existing flaws and relates to the formation of new flaws in a specimen, fracture toughness is a material property that measures the resistance to crack propagation from those flaws.[29,35] This resistance can be measured, but depends on the fracture mode of the material. Materials fail in one or more modes with mode I defined as pure tension, mode II as in-plane shear, and mode III as out-of-plane shear.[29] Figure 2.4 shows each of these modes schematically.

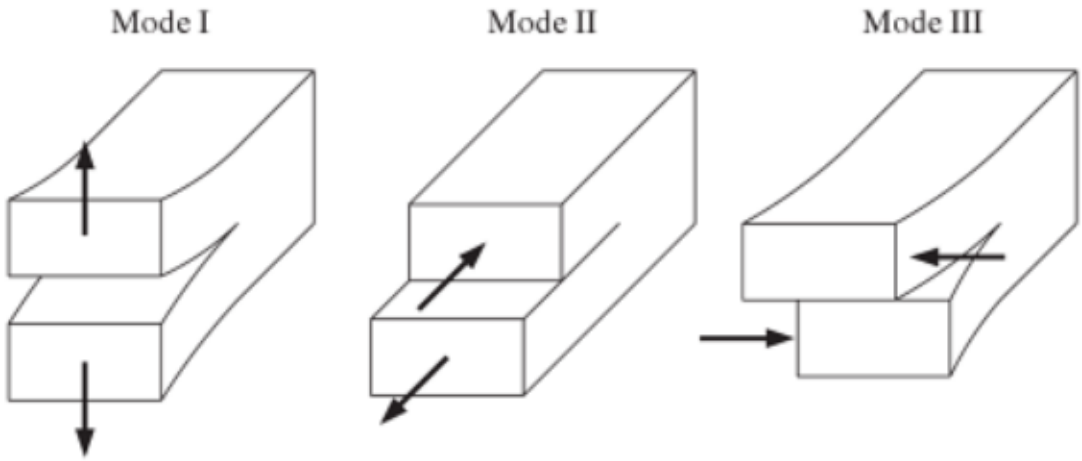

Figure 2.4. Schematic representation of fracture modes I, II, and III.[29]

Irwin used a general form of the Griffith theory to describe the driving force per unit area at a crack front.[42] Based on conservation of energy, Irwin defined the relationship for the energy needed to extend a crack using Equation 2.9, where G was defined by Irwin as the "force tendency", δl_i^{el} is the recoverable increment of strain energy of motion F_i, δU is the stored recoverable strain energy or potential energy, and

δA is the area of new surface produced by fracture.[42] A simplified version shown in Equation 2.10 reveals G to be the difference between mechanical work (δW) required to create a new surface and recoverable strain energy per unit of new surface area (δU) where both the work and stored energy are dependent on the load and change in crack length.[29] Equation 2.10 shows a release of energy per unit area or energy release rate, however, G is actually a measure of the energy available for incremental crack extension.[29,35]

$$G = \frac{\sum_i F_i \delta l_i^{el} - \delta U}{\delta A} \tag{2.9}$$

$$G = -\frac{\delta W - \delta U}{\delta A} \tag{2.10}$$

The compliance of the material will also change with an increase in crack length. As compliance and G are related through changes in crack length, G can be measured as a change in compliance with crack length. Irwin showed for plane stress conditions that when pure tensile stresses were applied to a central crack that G could be calculated using Equation 2.11 where σ is the applied stress, E is the Young's modulus, and 2a is a known crack length making "a" the half crack length.[42] A critical strain energy release rate, G_c, can be determined by substituting σ_f, failure stress, in for σ. When $G \geq G_c$, fracture occurs. The different strain energy release rates measured through Mode I, II, or III fracture can also be added to determine a G_{total}.

$$G = \frac{\pi \sigma^2 a}{E} \tag{2.11}$$

Irwin also modeled the stress on a component near a crack tip, represented two-dimensionally in Figure 2.5.[43] He showed that each stress is related by a constant K_I, and each is proportional to the distance r from the crack tip and the angle θ from the front of the crack tip.[43] The constant K_I, known as the mode I stress intensity factor, is related to G_I through the Young's modulus and can be calculated using Equation 2.12. Once K_I is known the entire stress field around a crack tip can be modeled. Knowing that some critical stress will cause a material to fail, a critical mode I stress intensity factor (K_{IC}) can also be determined and used to describe the fracture toughness of a material. Equation 2.13 shows how K_I can be determined for an infinite plate with a through thickness crack.[29,35]

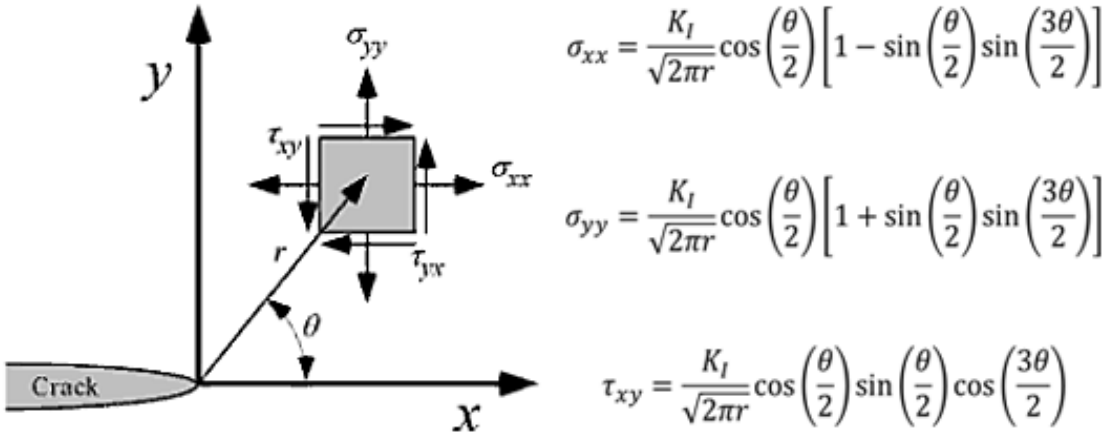

Figure 2.5. Element stresses at the tip of a propagating crack.[35]

$$G_I = \frac{K_I^2}{E} \tag{2.12}$$

$$K_I = \sigma\sqrt{\pi a} \tag{2.13}$$

While strain energy release rate is useful, K_{IC} is typically measured for ceramics due to the tendency of materials to fail in the mode that consumes the least amount of energy, which is mode I.[14,29,44-46] One drawback of using the stress intensity factor is that values cannot be added directly to produce a K_{total} as can be done with G_{total}. However, the K for each fracture mode can be converted into G for each mode and a G_{total} can be determined to describe the energy required to create new surfaces in mixed mode fracture.

Fracture toughness values for ceramics can be determined by several different methods.[29] Single edge notch beam and chevron notch beam tests require notching a specimen and testing in bending.[14,29,45] By notching, a known flaw size is present allowing for K_{IC} to be calculated based on the measured σ_c. Other methods utilize indentation to determine K_{IC}. The direct method of measuring K_{IC} through indentation is applied by indenting a material with enough force to produce radial/median cracks.[29,47] As the radial/median cracks form, K_I is initially greater than K_{IC} and the cracks propagate. As the cracks continue to propagate and lengthen, the stress at the crack tip will decrease. The crack will stop propagating when K_I has decreased below K_{IC}. The length of the radial/median cracks can be measured and Equation 2.14 can be used to determine K_{IC} where ξ is an empirically determined constant (0.016±0.004), 2c is the radial median crack length, and P is the load used to create the cracks.[47] Figure 2.6 shows an indent in a SiC ceramic containing 15 vol.% additions of TiB_2. The radial/median cracks can be seen emanating from the corners of the Vickers indent.

Measuring fracture toughness using the indirect method involves indenting a flexure bar to produce radial/median cracks and then breaking the bar. A modified indirect method involves indenting the bar multiple times. Failure will occur at the radial/median crack associated with one of the indents while the other indents remain on the verge of failure and K_{IC} can be determined based on the size of the their radial/median cracks.[29]

$$K_{IC} = \xi \left(\frac{E}{H}\right)^{\frac{1}{2}} \left(\frac{P}{c^{\frac{3}{2}}}\right) \tag{2.14}$$

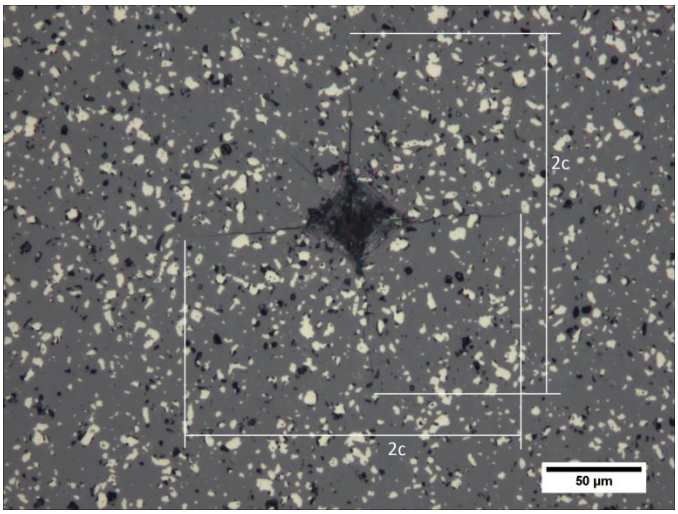

Figure 2.6. Radial/median cracks extending from the corners of a Vickers indent in SiC with 15 vol.% TiB_2 additions.

2.2.5 Weibull Modulus. Gaussian distributions are commonly used for statistically analyzing data sets. When analyzing data for ceramic materials, such as strength, Gaussian distributions fail to account for data that fall far from the mean. In brittle materials where a large flaw can have detrimental effects on strength, this is the

case.[48] W. Weibull proposed a material function based on the probability of failure for infinitely small volumes of material. In each volume slice, there is a chance of having a flaw or multiple flaws. Using specimens of the same volume effectively negates the effect of sample volume on strength, and thus the strength of the material is affected by the size and distribution of flaws.[29,48]

These flaws, designated "n", are like weak links in a chain. The chain fails at the weakest link, just like a brittle material fails at its largest flaw.[29,48,49] Weibull's material function is shown in Equation 2.15 where σ is the average failure strength/stress of a set of specimens, σ_o is the Weibull scale parameter, and m is the Weibull modulus.[48] The parameters m and σ_o are both unknown and must be determined empirically. The Weibull scale parameter, σ_o, is the stress required to put an amount of volume under stress that is equivalent to the mean volume fraction of flaws under stress. At this stress the mathematical probability of failure is 63% allowing σ_o to be determined from failure strength data.[48]

$$n(\sigma) = (\frac{\sigma}{\sigma_0})^m \tag{2.15}$$

The Weibull modulus "m" is determined by considering again that a specimen is made up of an infinite number of small slices where each of these slices has some probability of failure that is based on the material function. Weibull showed that this probability can be determined using Equation 2.16 where P_s is the probability of survival.[49,50] From empirical data, specimens are ranked from weakest to strongest. The rank (i) and total number of specimens are used to determine P_s using Equation 2.17,

which leaves m as the only unknown parameter.[29] The Weibull modulus can then be determined using a linear regression by plotting lnln(1/Ps) as a function of ln(σ) and fitting a line to the data. The slope of that line will be the Weibull modulus, m.[29] The Weibull modulus can then be used to compare different sets of data. Between different sets of data, a larger Weibull modulus indicates a narrower distribution of strengths for the specimens in that set and, therefore, a narrower distribution of flaw sizes.[29,49,50] Measured Weibull moduli of 8-17 have been reported for commercial armor ceramics making a Weibull modulus of over 10 a good mark for determining consistency between ceramic armors in a production lot or between production lots.[51]

$$P_s = -\exp(n(\sigma)) \tag{2.16}$$

$$P_s = 1 - (\frac{i-0.5}{n}) \tag{2.17}$$

2.3 MICROSTRUCTURAL EFFECTS ON MECHANICAL PROPERTIES

These mechanical properties: hardness, Young's modulus, fracture toughness, and strength each have their own significance when designing with ceramics for structural applications. The key to controlling each of these properties is control of the microstructure. Grain size, porosity, and second phases can all dramatically affect each of the aforementioned mechanical properties. In ceramic materials, it is generally accepted that hardness decreases with an increase in grain size.[27,52] Crystal anisotropy is one reason for this trend. An increase in grain size leads to an increase in the residual stress of the grains. These residual stresses can play a large role in how the material deforms when indented.[32,53,54] It is also typical to see a decrease in hardness with an

increase in fracture toughness.[29] Hilmas et al. reported an increase in the fracture toughness of SiC from 2.7 $MPa \cdot m^{1/2}$ to 9.2 $MPa \cdot m^{1/2}$ with additions of aluminum nitride (AlN) and Al_2O_3.[14] While fracture toughness increased, hardness decreased from 23 GPa to 15 GPa. The increase in fracture toughness was attributed to crack deflection around elongated SiC grains while the hardness drop may have been due a reduced work of indention that could have been caused by the presence of microcracks.[14,32] Based on analysis by Krell, the elongated SiC grains may have also played a part in the reduced hardness. Because of the brittle nature of ceramics, large grain sizes can act as strength limiting flaws that reduce the strength of the ceramic. Therefore, decreasing grain size effectively reduces the critical flaw size of a material and, in the absence of other, larger flaws, can lead to increased strength.[29] Porosity can affect each of these properties as well by acting as flaws, or reducing the work of indention during hardness measurements, or changing elastic wave propagation to affect Young's modulus.[29] The effects of second phases, specifically TiB_2 additions to SiC, will be discussed in Section 2.4.2 of this literature review. Because the microstructure of a ceramic affects its mechanical properties so drastically, microstructures must be evaluated to interpret mechanical property measurements.

2.4 SILICON CARBIDE-TITANIUM DIBORIDE CERAMIC COMPOSITES

2.4.1 Processing of SiC-TiB_2 Ceramics. SiC-TiB_2 ceramics can be produced using a variety of processing methods. The simplest method involves combining SiC and TiB_2 powders and densifying them through either hot-pressing or pressureless sintering.[55-58] To enhance densification, B_4C and C sintering aids are typically added to

react with and promote removal of oxide contamination from the surface of the powder particles.[59] For the reduction of SiO_2 that is present on the SiC particle surfaces, Reaction 1 can be utilized. Reduction of TiO_2 to TiB_2 follows Reaction 2. Another application for Reaction 2 is reaction sintering of SiC-TiB_2 composites by mixing SiC and TiO_2 powders with the appropriate amounts of B_4C and C to completely consume the oxygen in TiO_2 powder and converting it to TiB_2. This is sometimes done to achieve smaller TiB_2 particle sizes than is possible with readily available commercial TiB_2 powders.[15,60-62]

$$SiO_2 + 3C \rightarrow SiC + 2CO_{(g)} \quad (1)$$

$$2TiO_2 + B_4C + 3C \rightarrow 2TiB_2 + 4CO_{(g)} \quad (2)$$

The minimization of oxide content is an important step in densification of non-oxide ceramics. Due to the strong covalent bonding in materials like SiC and TiB_2, it is thought that the oxide layer hinders densification by reducing the surface energy of the grains while enhancing vapor transport and surface diffusion.[59,63-65] Vapor transport and surface diffusion are non-densifying sintering mechanisms, and act to coarsen grains, which inhibits densification (Figure 2.7).[66,67] Alliegro was the first to show SiC could be pressurelessly sintered using aluminum and iron sintering aids.[55,68] Prochazka, however, used B and C sintering aids for densification of SiC.[63] Prochazka showed that B segregated to the surface of SiC grains while C removed oxygen and reacted with free silicon impurities.[64] The segregation of B to the grain boundaries reduced the grain boundary energy and subsequently the ratio of grain boundary energy to surface energy,

γ_{gb}/γ_{sv}.[64] Removal of oxygen and free silicon also increased γ_{sv}, which further reduced γ_{gb}/γ_{sv}. For necking to occur, γ_{gb}/γ_{sv} must be less than $\sqrt{3}$. In contrast, when this ratio is greater than $\sqrt{3}$, grain boundary extension is halted and the closing of pores ceases.[64,69] Hence, reducing γ_{gb}/γ_{sv} is important for the enhancing densification during the sintering process.

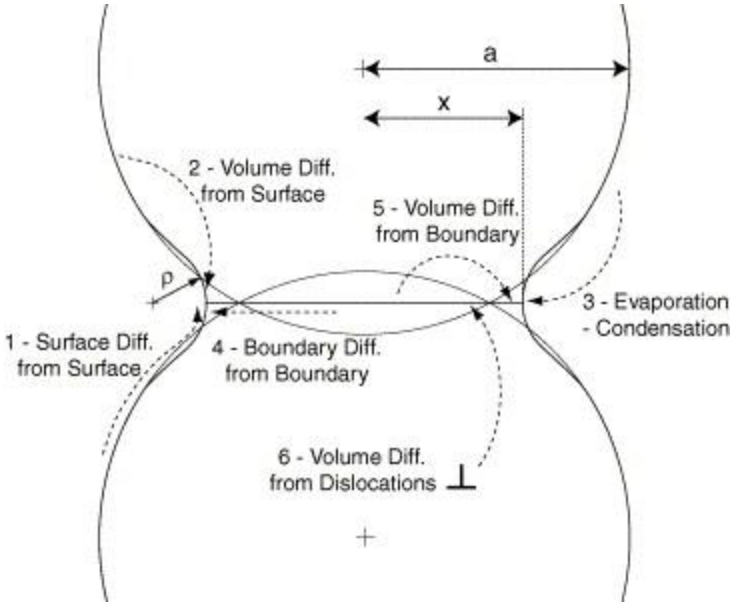

Figure 2.7. The six mechanisms of sintering. All the mechanisms lead to necking between particles, however, mechanisms 4-6 only lead to densification while mechanisms 1-3 lead to coarsening.[66]

Thermodynamic analysis of the reduction of TiO_2 supports the need for the addition of sintering aids. Since both Ti and B form stable solid oxides, TiO_2 and B_2O_3 are expected to form on the surface of TiB_2 powders based on the favorability of Reaction 3. However, B_2O_3 may hydrate in ambient conditions due to water vapor in the

atmosphere. A phase stability diagram (Figure 2.8) with axes of pH_2O and pO_2 at room temperature shows that the ambient laboratory conditions (star in Figure 2.8) under which powders are stored favor the formation of TiO_2 and HBO_2 rather than TiO_2 and B_2O_3. At room temperature (25^{o}C) under a vacuum of 27 Pa (hexagon in Figure 2.8), water can be removed, but HBO_2 still remains until a ~75 degree temperature increase. At 100^{o}C, enough water can be pulled from HBO2 to form B2O3 which subsequently melts a temperature of 500^{o}C.[70] A reaction between TiO_2, $B_2O_{3(l)}$, and C is then able to occur at ~1275^{o}C under a 27 Pa vacuum (Figure 2.9). However, a combination of C and B_4C sintering aids promotes the decomposition of TiO_2 at temperatures as low as ~1025^{o}C under the same 27 Pa vacuum. Excess B_2O_3 liquid can then be removed by evaporation at a temperature of ~1450^{o}C leaving powders that are nominally free of oxide impurities. As with SiC, the addition of C to TiB_2 enhances sintering by removing oxygen in the form of CO while B_4C removes oxygen and reacts with residual Ti to form TiB_2.[59]

$$4TiB_2 + 5O_{2\,(g)} \rightarrow 2TiO_2 + 2B_2O_3 \quad (3)$$

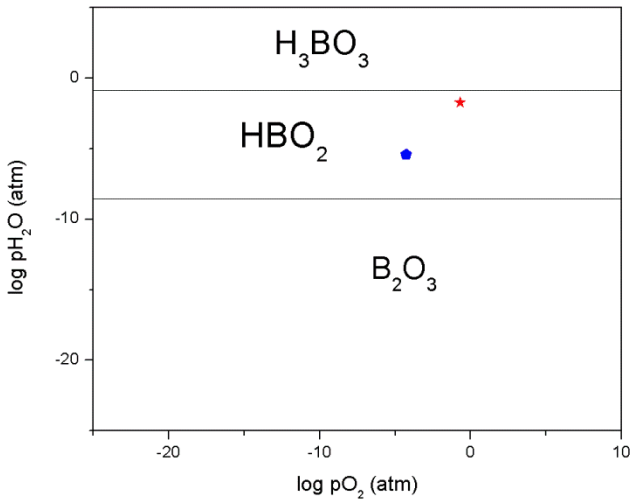

Figure 2.8. Phase stability diagram of B_2O_3, HBO_2 and H_3BO_3 at room temperature. Laboratory pH_2O/pO_2 is represented by the dot while furnace pH_2O/pO_2 is represented by the pentagon.

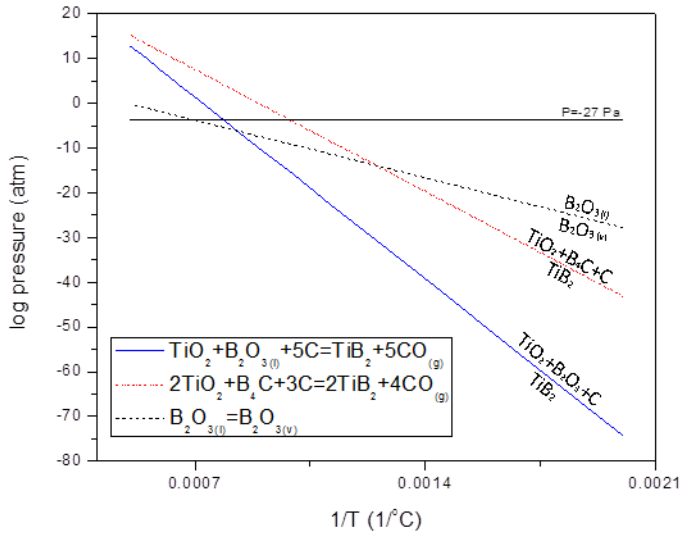

Figure 2.9. Phase stability diagram of the sintering aid reactions for reducing surface oxides on TiB_2 powders.

2.4.2 Properties of SiC-TiB_2 Ceramics. Silicon carbide (SiC) is a strong, hard, and chemically inert ceramic used in several applications that involve extreme environments.[13,71-74] The high hardness of SiC (20 to 27 GPa) makes it an attractive armor material.[12,18] However, SiC is brittle due to its low fracture toughness (2 to 5 $MPa \cdot m^{1/2}$), whereas high fracture toughness is desired for multi hit capability of the armor.[6,8,13,74] Improved fracture toughness is a goal for many researchers working with SiC ceramics. A fracture toughness of 6 to 9 $MPa \cdot m^{1/2}$ can be achieved by adding phases that promote crack propagation along the grain boundaries or by increasing the grain size; however, the hardness typically decreases as the fracture toughness increases. In some cases a drop in hardness of 5 to 10 GPa has been observed in SiC when the fracture toughness is increased 2 to 4 $MPa \cdot m^{1/2}$, an example of the classic hardness/toughness tradeoff.[6-8,14,75,76] Titanium diboride (TiB_2) also exhibits a high hardness (25-35 GPa) and it may overcome the hardness/toughness tradeoff when added as a particulate reinforcing phase to SiC.[9,15,77,78]

The addition of TiB_2 is expected to increase the hardness of SiC ceramics based on a volumetric rule of mixtures calculation. However, an increase in toughness is also expected due to thermal residual stresses within the SiC matrix. [77,78] SiC has a CTE along the c-direction of 4.45 x $10^{-6}/^{o}C$ compared to 8.6 x $10^{-6}/^{o}C$ for TiB_2. Along the a-direction, SiC has a CTE of 3.67 x $10^{-6}/^{o}C$ and TiB_2 has a value of 6.6 x $10^{-6}/^{o}C$.[9,79,80] The mismatch of CTE values puts the SiC matrix in compression and the TiB_2 particulate in tension for SiC-TiB_2 ceramics. This mismatch creates toughening due to the thermal residual stresses, which results in crack deflection as cracks running parallel to TiB_2 particles are drawn to the tensile stress field associated with the TiB_2 particles.[29] Because

of the expected boost in both hardness and fracture toughness, SiC-TiB_2 ceramics are attractive for armor applications.[15]

Previous studies have focused on the increase in toughness of SiC-TiB_2 composites due to thermal residual toughening, crack deflection, crack bridging, and microcracking.[36,77,78,81,82] Janney used indentation strength in bending to test the fracture toughness of SiC with 15 vol.% TiB_2, reporting a toughness of 4.5 MPa·$m^{1/2}$.[55] Using single edge notch beam testing, McMurtry reported a fracture toughness of 6.8 MPa·$m^{1/2}$ for SiC with 16 vol.% TiB_2.[56] Blanc showed the hardness/toughness tradeoff in a SiC matrix by adding different amounts of sub-micron TiB_2 particles. His results revealed that hardness decreased from 30 GPa to 23 GPa while toughness increased from 3.5 MPa·$m^{1/2}$ to 3.9 MPa·$m^{1/2}$ when TiB_2 content increased from 5 vol to 15vol.%.[15] More recently, Bucevac measured toughness using the indentation method for SiC-TiB_2 ceramics with varying amounts of TiB_2 particles that were formed in-situ. SiC with 12 vol.% TiB_2 had a toughness of 4.3 MPa·$m^{1/2}$ which increased to 5.3 MPa·$m^{1/2}$ for a TiB_2 content of 24 vol.%.[16] Using post-sintering heat treatments for grain growth, a maximum fracture toughness of 6.6 MPa·$m^{1/2}$ was later reported by Bucevac. Bucevac did not report how the increase in fracture toughness affected the materials hardness.[83]

PAPER

I. MICROSTRUCTURAL EFFECTS ON THE MECHANICAL PROPERTIES OF SiC-15VOL.% TiB_2 PARTICULATE REINFORCED CERAMIC COMPOSITES

Derek S. King, William G. Fahrenholtz, Greg E. Hilmas
Missouri University of Science and Technology
Materials Science and Engineering Dept.
1400 N. Bishop Ave.
Rolla, MO 65409

ABSTRACT

The microstructure and mechanical properties of SiC containing 15 vol.% of TiB_2 particulates were studied. The first, designated ST, was prepared from commercially available spray dried granules by hot pressing at 2225°C. The second, designated SiC-15TiB_2, was prepared from individual SiC and TiB_2 powders by hot-pressing at 2030°C. The average TiB_2 particle sizes were 5.7 μm for SiC-15TiB_2, which had a uniform distribution of TiB_2, and 4.5 μm for ST, which had a bimodal distribution of TiB_2 particle sizes. While the two ceramics both had hardness values of 26 GPa, the other properties were different. SiC-15TiB_2 had an average strength of 500 MPa compared to 350 MPa for ST. Likewise, a fracture toughness of 4.3 MPa·$m^{1/2}$ was measured for SiC-15TiB_2 and 3.1 MPa·$m^{1/2}$ for ST. In contrast, the Weibull modulus for the ST composite was 21 compared to 12 for SiC-15TiB_2. The average TiB_2 particle size for ST of 4.4 μm was above the threshold predicted for spontaneous microcracking. High resolution microstructural analysis showed that microcracking was present in ST, which accounted

for its higher Weibull modulus, but lower flexural strength, Young's modulus and fracture toughness compared to SiC-15TiB_2.

INTRODUCTION

Ceramics such as silicon carbide (SiC), aluminum oxide (Al_2O_3), and boron carbide (B_4C) are typically used in armor applications because of their high hardness.[1-3] For armor ceramics, the dwell time of a projectile at the interface of the armor system increases as hardness increases.[2] Typical hardness values for these common armor ceramics are 20 GPa to 27 GPa for SiC, 10 GPa to 15 GPa for Al_2O_3, and 30 GPa for B_4C.[1,4-6] Hauver introduced the concept of interface defeat, which was defined as the ability of a hard surface to stop a projectile and prevent penetration of the projectile into the underlying material.[7] Lundberg has shown that increased toughness of a confined ceramic increases the velocity needed to transition from interface defeat to penetration, also known as transition velocity.[4] Strength may also affect interface defeat. For projectiles travelling below the velocity needed to penetrate the ceramic, the ceramic retains a significant fraction of its original strength; however, above the penetration velocity the ceramics have no retained strength. [8] Strength and fracture toughness are also important for armor ceramics when multiple hit capability is desired.[9]

Many factors influence the ballistic performance of ceramics, so it is difficult to identify one property that is the key to a good armor system.[6] Instead of maximizing one particular property, qualification testing is used to ensure repeatability of a group of properties between different production lots. Gaussian distributions are commonly used for statistical analysis of data sets; however, Gaussian distributions do not account for

values that fall far from the mean, which can occur when analyzing the strength of brittle ceramics. Weibull used basic probability theories to address this shortcoming of Gaussian distributions.[10,11] For brittle materials, Weibull proposed a material function based on the probability of failure of a material with some number of flaws, designated "n", which act as possible weakest links. Equation 1 is a mathematical representation of the material function that Weibull proposed where σ is the failure strength/stress of a material, σ_0 is the Weibull scale parameter, and m is the Weibull modulus.[10] Both of the unknown parameters (σ_0, m) have physical significance. When a brittle specimen is loaded, stresses develop in a volume of material that increases as the load increases. If the volume of stressed material is equal to the mean volume of flaws, the probability of failure is equal to 63%. The stress at this probability is the Weibull scale parameter, or characteristic strength, σ_0. The Weibull modulus, m, can then be used to compare the flaw size distribution among different sets of data. A material with a higher Weibull modulus has a narrower flaw size distribution when compared to a similar material with a lower Weibull modulus.

$$n(\sigma) = (\frac{\sigma}{\sigma_0})^m \quad (1)$$

Silicon carbide-titanium diboride (SiC-TiB_2) ceramics are attractive for armor applications because they are both hard and tough compared to other ceramics.[12] Table I lists reported hardness and fracture toughness values for several commercial ceramic armor materials. For the silicon carbide-based armors listed, those with higher fracture toughness have lower hardness (i.e., an example of the classic property tradeoff). Ideally for armor applications, both of these properties would be maximized since hardness

increases dwell and fracture toughness enables multi-hit capability.[9] Ceramic composites with a particle reinforcing phase, like SiC with dispersed TiB_2 particles, provide the opportunity for toughening mechanisms such as microcracking, thermal residual toughening, crack branching, and crack deflection.[13-18] Many of these mechanisms arise due to differences in the thermal expansion coefficients between the matrix and reinforcing particles. Previous studies have focused on the increase in toughness of SiC-TiB_2 composites due to thermal residual toughening and microcracking. Janney used indentation strength in bending to test the fracture toughness of SiC with 15 vol.% TiB_2, reporting a toughness of 4.5 $MPa \cdot m^{1/2}$.[19] Using single edge notch beam testing, McMurtry reported a fracture toughness of 6.8 $MPa \cdot m^{1/2}$ for SiC with 16 vol.% TiB_2.[20] Blanc showed the hardness/toughness tradeoff in a SiC matrix by adding different amounts of sub-micron TiB_2 particles. His results revealed that hardness decreased from 30 GPa to 23 GPa while toughness increased from 3.5 $MPa \cdot m^{1/2}$ to 3.9 $MPa \cdot m^{1/2}$ when TiB_2 content increased from 5 to 15vol.%.[12] More recently, Bucevac measured toughness using the indentation method for SiC-TiB_2 ceramics with varying amounts of TiB_2 particles that were formed in-situ. SiC with 12 vol.% TiB_2 had a toughness of 4.3 $MPa \cdot m^{1/2}$ which increased to 5.3 $MPa \cdot m^{1/2}$ for a TiB_2 content of 24 vol.%.[18] Using post-sintering heat treatments for grain growth, a maximum fracture toughness of 6.6 $MPa \cdot m^{1/2}$ was later reported by Bucevac.[21]

The purpose of this paper is to evaluate the mechanical properties of two different SiC ceramics reinforced with 15 vol.% TiB_2. Two different starting powders were used to produce ceramics that had different microstructures. In addition, strengths of the resulting ceramics were compared using a two parameter Weibull analysis.

EXPERIMENTAL PROCEDURE

Two processing methods were utilized to produce SiC-TiB_2 composites containing nominally 15% TiB_2 by volume. A commercial source for SiC-TiB_2 (St. Gobain Ceramics; Hexoloy ST; Niagra Falls, NY) consisting of spray dried granules was used to produce hot-pressed billets designated as "ST". In addition, a second set of billets designated "SiC-15TiB_2" was produced from individual SiC (H.C. Starck; Grade UF-25; α-SiC; Newton, MA) and TiB_2 (Momentive; Grade HCT-F; Columbus, OH) powders. To promote densification of SiC-15TiB_2, 1 wt% B_4C (H.C. Starck; Grade HS) and sufficient phenolic resin (Georgia Pacific Chemicals, Atlanta, GA) to produce 2 wt.% C were mechanically mixed for two hours with the SiC and TiB_2 powders in a polyethylene jar using TiB_2 milling media in acetone. The resulting slurry was dried by rotary evaporation to minimize segregation of the constituents. The SiC-15TiB_2 powder was then ground and sieved to a -60 mesh before hot-pressing.

Billets nominally 55 mm by 55 mm by 5mm thick were hot pressed in a graphite element furnace (Thermal Technologies Inc., Model HP50-7010G, Santa Rosa, CA). A heating rate of 50^{o}C/min was used. Initially, the powder was heated under a vacuum of ~30 Pa (200 millitorr). Isothermal holds were employed at 1500^{o}C and 1700^{o}C to allow vacuum recovery as oxide contamination on the surfaces of the powder particles was removed as volatile species. At 1500^{o}C the isothermal hold time was 2 hours. The furnace was then held at 1700^{o}C until the chamber pressure returned to the nominal vacuum level of ~30 Pa. Before ramping to the final densification temperature, the furnace atmosphere was switched from vacuum to flowing argon. SiC-15TiB_2 powders were densified at 2030^{o}C with 32 MPa pressure. Pressing ceased when recorded ram

travel had stopped for a period of ten minutes. Hot pressing of ST was performed with the same ramp rate, isothermal hold temperatures, and pressure, except that the final hold temperature was 2225^{o}C. Loose ST granules, ~15 grams, were also sintered in furnace (Thermal Technologies Inc., Model 1000-4560-FP30) to 2175^{o}C without applied pressure.

The bulk density of all billets was measured using the Archimedes' method. Theoretical densities of 3.22, 4.52, 2.52, and 2.27 g/cm^3 and volume percents of 81.3, 14.4, 1.3, and 3.0 for SiC, TiB_2, B_4C and C, respectively, were used in calculating a volumetric rule of mixtures density of 3.37 g/cm^3. The billets were machined into mechanical test bars using an automated surface grinder (Chevalier Machinery Inc., Model FSG-3A818, Santa Fe Springs, CA) following the guidelines of ASTM C1161-02c for B-bars (3 mm by 4 mm by 45 mm) with a 600 grit surface finish. Specimens were tested in four point bending with a fully articulated fixture, using a screw-driven load frame (Instron, Model 5881, Norwood, MA) that was computer controlled (Instron, Bluehill 2, Norwood, MA). A total of 40 flexure bars of ST and 39 of SiC-15TiB_2 were tested to failure. The failure strengths of all of the test bars were included in the Weibull analysis. Applied load was measured using a 2 kN load cell and used to determine failure stress (σ). Strain was recorded from a deflectometer and used along with load to calculate Young's modulus (E). Two parameter Weibull distributions were calculated from the failure stresses. In addition to Young's modulus values determined from load-deflection curves, elastic constants were also determined using the impulse excitation method (Grindosonic Mk5 Industrial, J.W. Lemmens Inc., Heverlee, Belgium) following ASTM C1259-08e1.

Vickers' hardness was measured (Struers Inc., Duramin 5, Cleveland, OH) using a load of 1 kg with a 15 s dwell time. Reported values were an average of 10 hardness indents. Hardness specimens were prepared by mounting sections of broken flexure bars in an epoxy resin and polishing to a mirror finish using successively finer diamond abrasives down to 0.25 μm. Fracture toughness was determined using direct crack measurements. Specimens were indented (Leco Corporation, Model V-100-A2, St. Joseph, MI) with a load of 5 kg on a polished surface with a Vickers diamond tip followed by measurement of the length of radial median cracks formed during indentation.[22]

Using broken flexure bars, microscopy of polished specimens was performed using both optical (Epiphot 200, Nikon, Tokyo, Japan) and scanning electron microscopes (S-570, Hitachi, Tokyo Japan and Helios Nanolab 600, FEI, Hillsboro, OR). Area fractions of the constituent phases and porosity were determined using computer image analysis (ImageJ, National Institutes of Health, Bethesda, MD). Particle size was determined by equating average particle area to the area of a sphere with equivalent diameter. Chemical analysis was performed using energy dispersive spectroscopy (Sirius SD, SGX Sensortech Ltd., Wooburn Green, England) in combination with Revolution software (4pi Analysis Inc., Hillsborough, NC). In addition to the dense billets, loose, sintered ST granules were cross-sectioned for microscopy by covering the bottom of a 1.25 in. epoxy mount with a layer of sintered granules, mounting in epoxy and grinding. Once cross-sectioned, the granules were polished using successively finer diamond abrasives down to 0.25 μm.

RESULTS AND DISCUSSION

Hot pressing produced dense specimens for both compositions. Bulk densities were 3.37 g/cm^3 for both ST and SiC-15TiB_2 (Table II). SEM micrographs (Figure 1) confirmed that both ST and SiC-15TiB_2 were nearly fully dense. Most of the dark areas in the images were either B_4C or C, which were added as sintering aids. A limited number of pores were visible. Some pores were trapped within TiB_2 grains while others were in the SiC matrix. The area fraction of porosity calculated using computerized image analysis was less than 1 vol.%. Hence, both composites were considered to be fully dense and porosity was not considered to have a significant impact on the measured properties of the two materials.

Microstructural information obtained using scanning electron microscopy showed that TiB_2 distribution differed between the two materials. Figure 1 gives a side-by-side comparison of ST (1a) and SiC-15TiB_2 (1b), cut perpendicular to the hot pressing direction. The area fraction of TiB_2 was 12.1% for ST and 15.3% for SiC-15TiB_2. Based on the average area of TiB_2 particles, the equivalent circular diameters for the isolated TiB_2 regions were 2.3 μm for ST and 2.7 μm for SiC-15TiB_2. Measured densities were consistent with TiB_2 contents of 15 vol.% for both composites, assuming full density. However, in the case of ST, agglomeration of TiB_2 particles led to a bimodal distribution of TiB_2 particle sizes, which is apparent in Figure 1a with some larger (~5 μm diameter) and some smaller (<1 μm diameter) particles. To determine the cause of agglomeration, cross sections of sintered ST granules were examined using SEM (Figures 2). The cross sections and EDS map show that TiB_2 segregated to the outer surface of the spray dried ST granules. While both composites had nominally identical amounts of TiB_2 and

similar average TiB_2 particle sizes, SiC-15TiB_2 (Figure 1b) had a more uniform distribution of the TiB_2 particulate phase compared to ST (Figure 1a).

The structure of the spray dried granules was retained in the ST ceramics after hot pressing. Figure 3 shows an optical micrograph of a cross section of an ST ceramic that was cut perpendicular to the hot pressing direction. The image shows light colored features on the order of 70 μm in diameter, which are the remnants of the spray dried granules. As shown in Figure 2, TiB_2 was segregated to the outside of the granules prior to hot pressing and this distribution was maintained through the hot pressing process. However, the uniform starting granule size led to the development of a microstructure with a regular TiB_2 distribution indicative of the segregation in the spray dried granules.

Table II summarizes the mechanical properties of the two different ceramic materials. The Vickers hardness values for both ceramics were ~26 GPa when measured with an indentation load of 1 kg. Based on hardness values of 33 GPa for TiB_2 and 27 GPa for SiC, a volumetric rule of mixtures calculation predicts a composite hardness value of 28 GPa for SiC containing 15 vol.% TiB_2.[5] In general, hardness values are affected by factors such as grain size, the presence of grain boundary phases, porosity, and processing conditions. Microcracking can also affect measured hardness values. For materials with anisotropic crystal structures (i.e., hexagonal TiB_2 or SiC) microcracking can develop due to residual thermal stresses.[23-25] In SiC-TiB_2, microcracking can also result from the residual thermal stresses that develop during cooling from the densification temperature due to the difference in the coefficient of thermal expansion (CTE) values of the two constituents. The CTE along the c-direction for SiC and TiB_2

are 4.45 x $10^{-6}/^{o}$C and 8.6 x $10^{-6}/^{o}$C, respectively. In the a-direction, SiC has a CTE of 3.67 x $10^{-6}/^{o}$C and TiB_2 has a value of 6.6 x $10^{-6}/^{o}$C.[24,26,27] Despite hardness values that are lower than expected based on a rule of mixtures calculation, the composite hardness of 26 GPa is still higher than reported for many typical ceramic armors (Table I).[1,2]

Young's modulus values were calculated from stress-strain curves for ST and SiC-15TiB_2. The modulus of SiC-15TiB_2 was 458±21 GPa, which was higher than the value of 417±13 GPa, that was determined for ST. Elastic constants were also measured using impulse excitation testing with Young's modulus values determined to be 465±4 GPa for SiC-15 TiB_2 and 433±5 GPa for ST. Using a volumetric rule of mixtures calculation and assuming values of 450 GPa for SiC and 560 GPa for TiB_2, the predicted Young's modulus value was 467 GPa for both materials.[24,28] Hence, the Young's modulus of SiC-15TiB_2 determined by both methods was close to the expected value, while the value for the ST ceramics was lower than expected. Gu and Faber observed a similar drop in measured Young's modulus for a SiC-TiB_2 ceramic.[13] Their analysis of the stress-strain behavior in tensile testing revealed non-linear behavior and a drop in Young's modulus, which was attributed to microcracking in their material. For the present study, non-linear behavior was not observed in the load-deflection curves generated during flexure testing, but the Young's modulus of the ST ceramic was lower than expected, which might be an indication of microcracking in that material.

The average flexural strengths were 380 MPa for ST and 500 MPa for SiC-15TiB_2. In addition, Weibull analysis was used to determine characteristic strengths where the probability of survival was 37% based on original work by Weibull.[10] The

characteristic strengths were similar to the average strengths at 390 MPa for ST and 520 MPa for SiC-15TiB_2. The SiC-15TiB_2 composite had a higher strength than ST, but the linear regression fit of the strength data in Figure 4 showed that the Weibull modulus of ST was 21 compared to 12 for SiC-15TiB_2. The higher Weibull modulus indicates a tighter statistical grouping of strengths for ST, but does not provide insight into why the strength distribution was narrower. The uniform granule distribution shown in Figure 3 may contribute to the increase in Weibull modulus since a more regular microstructure would lead to a more uniform distribution of flaw sizes.[29] So, the higher Weibull modulus of ST indicates a narrower distribution of flaw sizes, but the lower average strength means that the average critical flaw size is larger for ST than for SiC-15TiB_2.

SiC-15TiB_2 had a fracture toughness of 4.3 $MPa \cdot m^{1/2}$, which was about 30% higher than the value of 3.1 $MPa \cdot m^{1/2}$ measured for ST. For SiC armors with a similar hardness (Table I) the toughness of both ST and SiC-15TiB_2 remained higher while retaining hardness above 25 GPa. The equations of Taya et al. can be used to estimate the toughening effect of particulate composite ceramics due to thermal residual stresses that arise from differences in the CTE values of the constituent phases.[15] The stress value in the SiC matrix was calculated to be -350 MPa (compressive) while a stress of 1975 MPa (tensile) was estimated in the TiB_2 particulate phase. The average particle spacing (λ), which is illustrated in Figure 5, was calculated using Equation 2 where d_p is the average particle diameter and ϕ_F is the volume fraction of particles.[30] Then, λ was combined with the average matrix stress to estimate the toughening due to thermal residual stresses using Equation 3.[15]

$$\lambda = d_p \left[\left(\frac{\pi}{6\phi_F}\right)^{\frac{1}{3}} - 1 \right] \quad (2)$$

$$\Delta K_I = 2q\sqrt{\frac{2(\lambda)}{\pi}} \quad (3)$$

The changes in toughening (ΔK_I) for SiC-15TiB_2 and ST were calculated to be -0.66 and -0.60 MPa·$m^{1/2}$, respectively. Since TiB_2 acts to pin the grain growth in SiC, the toughness of the matrix would be expected to be similar to the toughness of a fine grained (~110 nm) SiC with no sintering aids, which was reported to be ~2 MPa·$m^{1/2}$.[31] Assuming this value of 2 MPa·$m^{1/2}$ to be the baseline for the matrix in the current study, SiC-15TiB_2 has a toughness that is 2.3 MPa·$m^{1/2}$ higher than the matrix while the toughness of ST is 1.1 MPa·$m^{1/2}$ higher than the matrix. Therefore, the residual thermal stress would only increase fracture toughness from ~2 MPa·$m^{1/2}$ for pure SiC to ~2.6 MPa·$m^{1/2}$ for the composites. Since the composite toughening for SiC-15TiB_2 was ~2.3 MPa·$m^{1/2}$ compared to fine-grained SiC ceramics, toughening due to thermal residual stresses was not the only toughening mechanism operating in SiC-TiB_2 composites. Figure 6 also shows a crack extending from the end of an indentation in SiC-15TiB_2, which appears to deflect around TiB_2 particles. In addition, the crack appears to branch within a larger TiB_2 particle. While crack deflection and bridging increase toughness compared to fine-grained SiC, they should provide similar increases in toughness for both ST and SiC-15TiB_2.[12,32] Hence, some other mechanism is needed to explain the differences in toughness values between the ST and SiC-15TiB_2 ceramics. Elucidation of the reason for the difference in toughness may also explain the drop in strength and increase in Weibull modulus for ST compared to SiC-15TiB_2.

Microcracking has previously been cited as a toughening mechanism in SiC-TiB_2 ceramics.[13,16,18] If present, microcracks may render other toughening mechanisms like thermal residual toughening ineffective by releasing some or all of the residual stresses when the cracks are formed.[33] The lower than expected values for Young's modulus and strength, combined with the increases in fracture toughness and Weibull modulus, may also indicate the presence of microcracking in the ST composite.[34,35] To compare toughening due to crack deflection in ST and SiC-15TiB_2, the angles of each of the crack deflections occurring in the four radial median cracks from one of the Vickers indents obtained using a 5 kg load were measured. SiC-15TiB_2 had an average angle of deflection of $29^o \pm 19^o$ from a total of 53 deflections. Similarly, ST had an average deflection angle of $25^o \pm 16^o$ from a total of 33 deflections. The difference in the number of deflections is likely due to the difference in TiB_2 distribution as SiC-15TiB_2 had a more uniform distribution of dispersed TiB_2 particulate while ST contained larger agglomerates or clusters of TiB_2 grains. In addition, the TiB_2 agglomerates were distributed at a larger path length of ~70 μm on average (Figure 3). In ST, the larger TiB_2 agglomerates acted like larger TiB_2 particles. Based on the calculations of Magley, microcracking is expected to occur for TiB_2 particle sizes over 4.4 μm.[36] Because the average TiB_2 particle size for ST and SiC-15TiB_2 are below the calculated value for spontaneous microcracking, microcracking would not be expected in either ceramics. However, large TiB_2 particles were not observed in SiC-15TiB_2 due to the uniform TiB_2 distribution. SEM analysis shown in Figure 7 confirmed that microcracking was present in the ST ceramic. Both circumferential/ring microcracks and radial microcracks were observed, which would release tensile thermal residual stresses. While circumferential

microcracking can boost toughness in a stress-free matrix, radial microcracks can lead to larger inherent flaw sizes, which can reduce the strength of the material.[29,37]

Crack tip shielding through transformation or microcrack toughening act as mechanisms that reduce the driving force at the tip of a propagating crack. Because of this, the driving force of the crack must be increased to sustain cracking as crack length increases.[38] In other words, materials with microcracks can exhibit R-curve behavior. Gu and Faber noted that in a SiC-TiB_2 ceramic with a non-uniform TiB_2 particle size distribution that localized changes in fracture toughness as a crack advanced through the areas of differing stress states could give rise to R-curve behavior.[16] While R-curve testing was not performed in the present study, the presence of microcracking and the bimodal TiB_2 distribution showed that the ST composite had characteristics similar to materials that exhibit R-curve behavior. In turn, R-curve behavior contributes to an increase in the Weibull modulus by reducing the distribution of strengths.[29,39-42] The combination of the uniform granule size distribution and microcracking in the ST ceramic boosted the Weibull modulus, while decreasing strength and Young's modulus compared to SiC-15TiB_2, which had a uniform distribution of TiB_2 particles.

CONCLUSIONS

Two different SiC ceramics containing nominally 15 vol.% TiB_2 were produced using different green processing techniques and both were densified by hot-pressing. Commercially available spray dried granules (ST) and a mixture of SiC-TiB_2 (SiC-15TiB_2) had the same Vickers hardness of 26 GPa. Both ceramics also exhibited higher fracture toughness values compared to other high hardness ceramic armor materials. The

Young's modulus for SiC-15TiB_2 was 465 GPa, which matched well with a value of 467 GPa predicted for the nominal composition using a rule of mixtures calculation. However, the Young's modulus of ST was lower, 433 GPa. Weibull analysis of strength data showed that the average strength of SiC-15TiB_2 was 500 MPa, which was higher than the strength of ST (380 MPa). The Weibull moduli of the SiC-15TiB_2 and ST composites were determined to be 12 and 21, respectively. Toughness measured using the direct crack method resulted in a toughness of 4.3 $MPa \cdot m^{1/2}$ for SiC-15TiB_2, which was ~30% higher than ST at 3.1 $MPa \cdot m^{1/2}$ even though both composites contained the same amount of TiB_2. A decrease in both strength and Young's modulus, along with an increase in Weibull modulus, indicated that microcracking was likely to be present within the ST ceramic. High resolution SEM analysis was used to verify the presence of microcracking in the ST composite. Microcracking likely released tensile thermal residual stresses in the TiB_2 particles and lowered the toughness of ST compared to SiC-15TiB_2. Combined with a regular architecture, microcracking led to a narrower flaw size distribution and a concomitant higher Weibull modulus in the ST ceramic compared to SiC-15TiB_2.

ACKNOWLEDGEMENTS

Research was sponsored by Saint-Gobain Ceramics and the Army Research Laboratory and was accomplished under Cooperative Agreement Number W911NF-08-2-0001. The views and conclusions contained in this document are those of the authors and should not be interpreted as representing the official policies, either expressed or

REFERENCES

[1]M. Flinders, D. Ray, A. Anderson, and R. A. Cutler, "High-Toughness Silicon Carbide as Armor," *J. Am. Ceram. Soc.*, **88**[8] 2217-26 (2005).

[2]D. Ray, M. Flinders, A. Anderson, and R. A. Cutler, "Hardness/Toughness Relationship for SiC Armor," pp. 401-10. in 27th Annual Cocoa Beach Conference on Advanced Ceramics and Composites: A: Ceramic Engineering and Science Proceedings**.** John Wiley & Sons, Inc., 2008.

[3]W. G. Fahrenholtz, E. W. Neuman, H. J. Brown-Shaklee, and G. E. Hilmas, "Superhard Boride–Carbide Particulate Composites," *J. Am. Ceram. Soc.*, **93**[11] 3580-83 (2010).

[4]P. Lundberg and B. Lundberg, "Transition between interface defeat and penetration for tungsten projectiles and four silicon carbide materials," *Int. J. Impact Eng.*, **31**[7] 781-92 (2005).

[5]"Engineered Materials Handbook: Ceramics and Glasses," **Vol. 4**. ASM International, (1991).

[6]B. Matchen, "Applications of Ceramics in Armor Products," *Key Eng. Mater.*, **122-124** 333-44 (1996).

[7]G. E. Hauver, "The Ballistic Performance of Ceramic Targets," pp. 23-34 in Army Symposium of Solid Mechanics. (1993).

[8]P. Lundberg, Renstrom, and B. Lundberg, "Impact of metallic projectiles on ceramic targets: transition between interface defeat and penetration," *Int. J. Impact Eng.*, **24** 259-75 (2000).

[9]P. G. Karandikar, G. Evans, S. Wong, M. K. Aghajanian, and M. Sennett, "A Review of Ceramics for Armor Applications," pp. 163-75. in Advances in Ceramic Armor IV: Ceramic Engineering and Science Proceedings, Volume 29, Issue 6**.** John Wiley & Sons, Inc., 2009.

[10]W. Weibull, "A Statistical Theory of the Strength of Materials." in**.** Royal Technical University, Stockholm, 1939.

[11]W. Weibull, "A Statistical Distribution Function of Wide Applicability," *J. App. Mech.*, **18** 293-97 (1951).

[12]C. Blanc, F. Thevenot, and D. Goeuriot, "Microstructural and mechanical characterization of SiC-submicron TiB_2 composites," *J. Eur. Ceram. Soc.*, **19**[5] 561-69 (1999).

[13]W. H. Gu and K. T. Faber, "Tensile Behavior of Microcracking SiC-TiB_2 Composites," *J. Am. Ceram. Soc.,* **78**[6] 1507-12 (1995).

[14]M.-J. Pan, P. A. Hoffman, D. J. Green, and J. R. Hellmann, "Elastic Properties and Microcracking Behavior of Particulate Titanium Diboride-Silicon Carbide Composites," *J. Am. Ceram. Soc.,* **80**[3] 692-98 (1997).

[15]M. Taya, S. Hayashi, A. S. Kobayashi, and H. S. Yoon, "Toughening of a Particulate-Reinforced Ceramic-Matrix Composite by Thermal Residual Stress," *J. Am. Ceram. Soc.,* **73**[5] 1382-91 (1990).

[16]W. H. Gu, K. T. Faber, and R. W. Steinbrech, "Microcracking and R-curve behavior in SiC-TiB_2 composites," *Acta Metall. Mater.,* **40**[11] 3121-28 (1992).

[17]D.-H. Kuo and W. M. Kriven, "Mechanical behavior and microstructure of SiC and SiC/TiB_2 ceramics," *J. Eur. Ceram. Soc.,* **18**[1] 51-57 (1998).

[18]D. Bucevac, S. Boskovic, B. Matovic, and V. Krstic, "Toughening of SiC matrix with in-situ created TiB_2 particles," *Ceram. Int.,* **36**[7] 2181-88 (2010).

[19]M. A. Janney, "Mechanical Properties and Oxidation Behavior of Hot-Pressed SiC-15vol%-TiB_2 Composite," *Bull. Am. Ceram. Soc.,* **66**[2] 322-24 (1987).

[20]C. H. McMurtry, W. D. G. Boecker, S. G. Seshadri, J. S. Zanghi, and J. E. Garnier, "Microstrutcture and Material Properties of SiC-TiB_2 Composites," *Bull. Am. Ceram. Soc.,* **66**[21] 325-29 (1987).

[21]D. Bucevac, B. Matovic, B. Babic, and V. Krstic, "Effect of post-sintering heat treatment on mechanical properties and microstructure of SiC–TiB_2 composites," *Mater. Sci. Eng., A,* **528**[4–5] 2034-41 (2011).

[22]G. R. Anstis, P. Chantikul, B. R. Lawn, and D. B. Marshall, "A Critical Evaluation of Indentation Techniques for Measuring Fracture Toughness: I, Direct Crack Measurements," *J. Am. Ceram. Soc.,* **64**[9] 533-38 (1981).

[23]T. S. Srivatsan, G. Guruprasad, D. Black, R. Radhakrishnan, and T. S. Sudarshan, "Influence of TiB_2 content on microstructure and hardness of TiB_2–B_4C composite," *Powder Technol.,* **159**[3] 161-67 (2005).

[24]B. Basu, "Processing and Properties of Monolithic TiB_2 Based Materials," *Int. Mater. Rev.,* **51**[6] 352-74 (2006).

[25]D. A. Ray, S. Kaur, R. A. Cutler, and D. K. Shetty, "Effects of Additives on the Pressure-Assisted Densification and Properties of Silicon Carbide," *J. Am. Ceram. Soc.,* **91**[7] 2163-69 (2008).

[26]Z. Li and R. C. Bradt, "Thermal Expansion and Thermal Expansion Anisotropy of SiC Polytypes," *J. Am. Ceram. Soc.,* **70**[7] 445-48 (1987).

[27]M. K. Ferber, P. F. Becher, and C. B. Finch, "Effect of Microstructure on the Properties of TiB_2 Ceramics," *J. Am. Ceram. Soc.,* **66**[1] C-2-C-3 (1983).

[28]P. T. B. Shaffer and C. K. Jun, "The elastic modulus of dense polycrystalline silicon carbide," *Mater. Res. Bull.,* **7**[1] 63-69 (1972).

[29]J. B. Wachtman, W. R. Cannon, and M. J. Matthewson, "Mechanical Properties of Ceramics," 2nd ed. John Wiley & Sons, Inc.: Hoboken, NJ, (2009).

[30]S. Matteucci, V. A. Kusuma, D. Sanders, S. Swinnea, and B. D. Freeman, "Gas transport in TiO_2 nanoparticle-filled poly(1-trimethylsilyl-1-propyne)," *J. Membr. Sci.,* **307**[2] 196-217 (2008).

[31]Y.-W. Kim, M. Mitomo, and H. Hirotsuru, "Grain Growth and Fracture Toughness of Fine-Grained Silicon Carbide Ceramics," *J. Am. Ceram. Soc.,* **78**[11] 3145-48 (1995).

[32]K.-S. Cho, H.-J. Choi, J.-G. Lee, and Y.-W. Kim, "In situ enhancement of toughness of SiC-TiB_2 composites," *J. Mater. Sci.,* **33**[1] 211-14 (1998).

[33]A. G. Evans and K. T. Faber, "Crack-Growth Resistance of Microcracking Brittle Materials," *J. Am. Ceram. Soc.,* **67**[4] 255-60 (1984).

[34]G. C. Reilly and J. D. Currey, "The effects of damage and microcracking on the impact strength of bone," *J. Biomech.,* **33**[3] 337-43 (2000).

[35]V. Skorokhod and V. D. Krstic, "High strength-high toughness B_4C-TiB_2 composites," *J. Mater. Sci. Lett.,* **19**[3] 237-39 (2000).

[36]D. J. Magley, R. A. Winholtz, and K. T. Faber, "Residual Stress in a Two-Phase Microcracking Ceramic," *J. Am. Ceram. Soc.,* **76**[3] 1641-44 (1990).

[37]A. G. Evans and K. T. Faber, "Toughening of Ceramics by Circumferential Microcracking," *J. Am. Ceram. Soc.,* **64**[7] 394-98 (1981).

[38]R. O. Ritchie, "Mechanisms of fatigue crack propagation in metals, ceramics and composites: Role of crack tip shielding," *Mater. Sci. Eng., A,* **103**[1] 15-28 (1988).

[39]J. Gong, W. Si, and Z. Guan, "Weibull modulus of fracture strength of toughened ceramics subjected to small-scale contacts," *J. Mater. Sci.,* **36**[10] 2391-96 (2001).

[40]D. K. Shetty and J.-S. Wang, "Crack Stability and Strength Distribution of Ceramics That Exhibit Rising Crack-Growth-Resistance (R-Curve) Behavior," *J. Am. Ceram. Soc.*, **72**[7] 1158-62 (1989).

[41]R. F. Cook and D. R. Clarke, "Fracture stability, R-curves and strength variability," *Acta Metall. Mater.*, **36**[3] 555-62 (1988).

[42]S. Kaur, D. K. Shetty, and R. A. Cutler, "R Curves and Crack-Stability Map: Application to Ce-TZP/Al_2O_3," *J. Am. Ceram. Soc.*, **90**[11] 3554-58 (2007).

Table I: Reported Hardness and Fracture Toughness Values for Common Armor Ceramics

Material	Hardness (GPa)	Fracture Toughness ($MPa \cdot m^{1/2}$)
SiC-B (Cercom)[1]	20.6±1.2	5.0±0.5
SC-RB (CoorsTek)	24.5	3-4
SiC-N[4]	27.16±1.76	2.75±0.32
SiC-SC-1RN[4]	28.85±1.92	2.84±0.22
CAP 3 (CoorsTek)	14.1	4-5

Table II: Summary of Density and Mechanical Properties of ST and SiC-15TiB_2 Ceramics

Composite	Bulk Density (g/cm^3)	Relative Density (%)	Strength (MPa)	Young's Modulus, Stress/strain (GPa)	Young's Modulus, Impulse (GPa)	Hardness (GPa)	Fracture Toughness ($MPa \cdot m^{1/2}$)
ST	3.37	<99%	379±21	417±16	430	25.7±1.1	3.1±0.2
SiC-15TiB_2	3.37	<99%	499±48	458±21	468	26.0±1.8	4.3±0.4

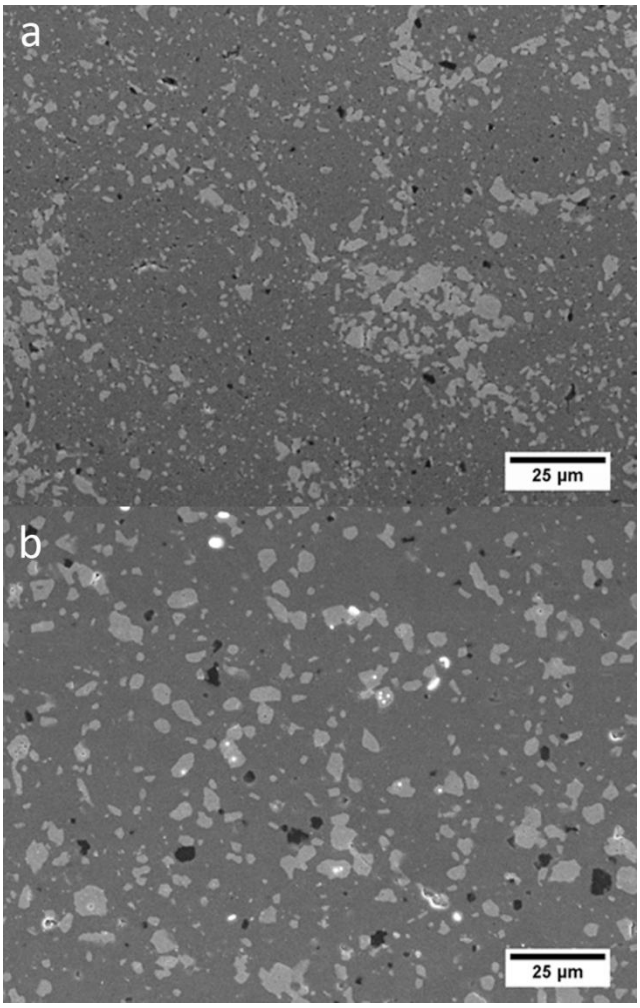

Figure 1. Cross sections perpendicular to the hot-pressing direction of (a) ST and (b) and SiC-15TiB_2 revealing the individual phases of TiB_2 (light grey), SiC (dark grey), and B_4C/C/pores (black).

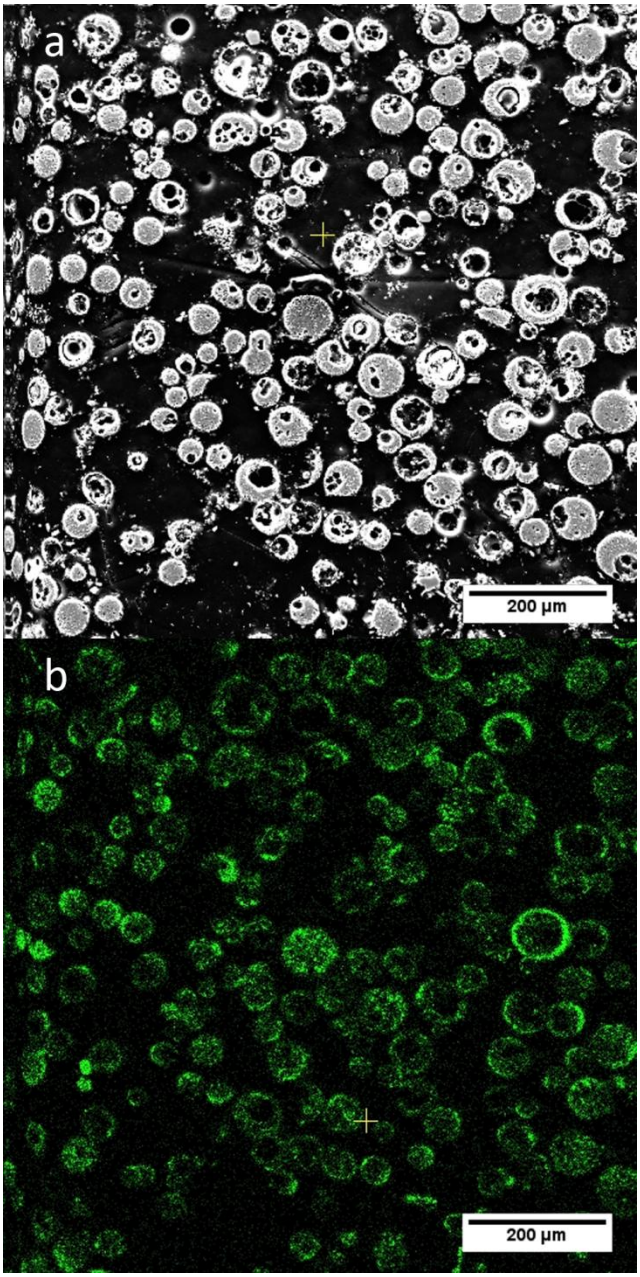

Figure 2. SEM image of sintered ST spray dried granules (a) and accompanying EDS phase mapping showing Ti dispersion in spray dried ST granules (b).

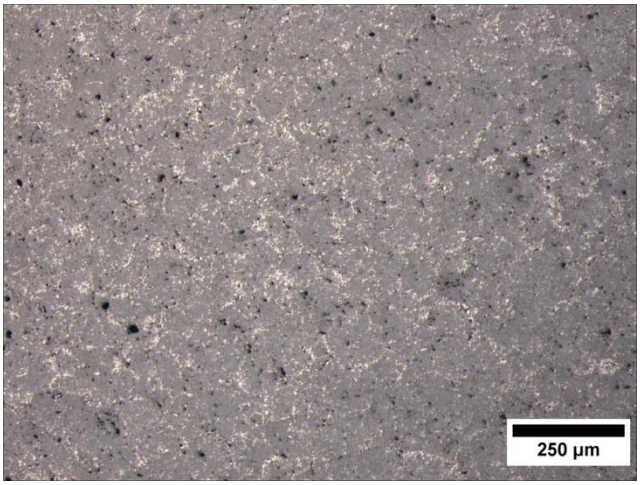

Figure 3. Optical micrograph of an ST billet perpendicular to the hot pressing direction showing that TiB_2 (lighter contrast) is preferentially distributed around SiC-rich regions.

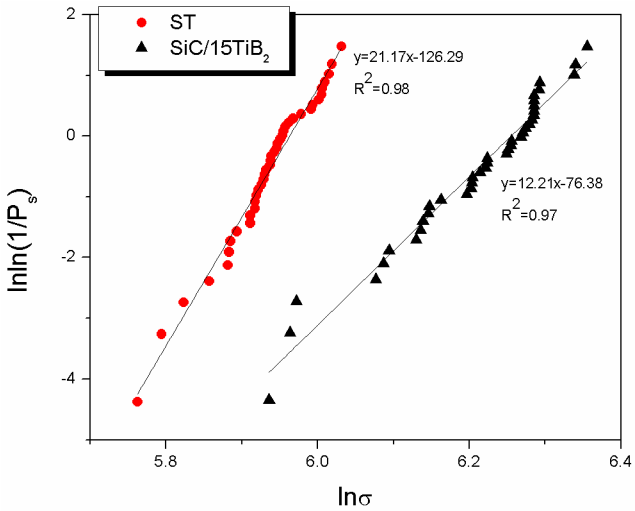

Figure 4. Weibull analysis of the ST and SiC-15TiB_2 composites where the characteristic strengths were 390 and 520 MPa and the Weibull moduli were 21 and 12, respectively. Average strengths were 380 for ST and 500 MPa for SiC-15TiB_2.

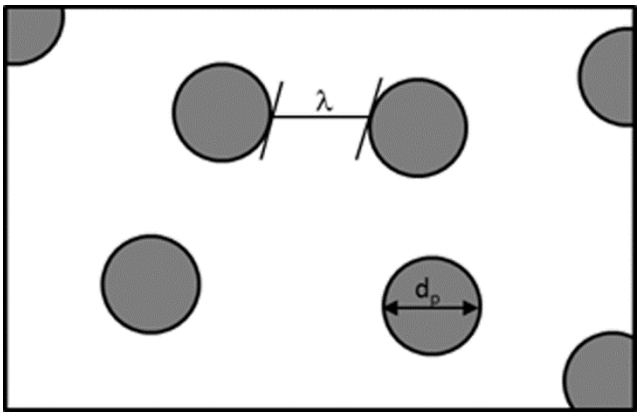

Figure 5. Schematic of particles dispersed in a matrix showing the particle diameter (d_p) and interparticle spacing (λ).

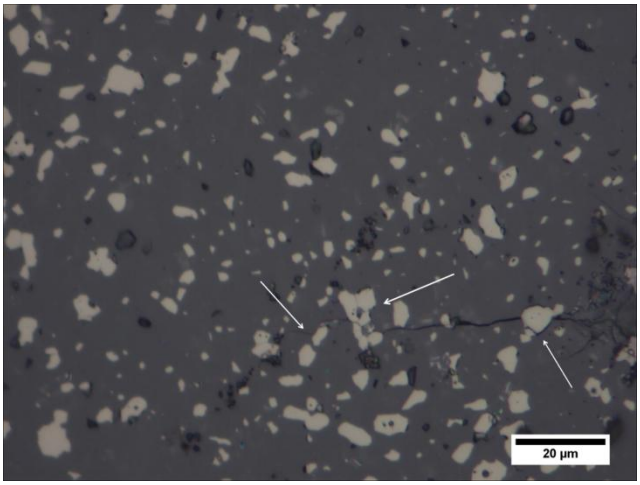

Figure 6. Radial median crack extending from the end of an indent showing crack deflection around TiB_2 particles and crack branching within TiB_2 particles.

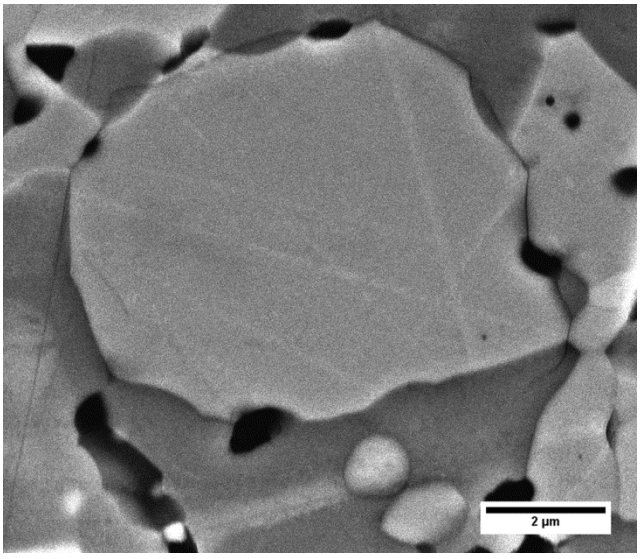

Figure 7. SEM image showing a circumferential microcrack around a TiB_2 particle running through both the particle and the SiC matrix.

II. SILICON CARBIDE-TITANIUM DIBORIDE CERAMIC COMPOSITES

Derek S. King, William G. Fahrenholtz, Greg E. Hilmas
Missouri University of Science and Technology
Materials Science and Engineering Dept.
1400 N. Bishop Ave.
Rolla, MO 65409

ABSTRACT

The effect of TiB_2 content on mechanical properties of silicon carbide-titanium diboride ceramic composites was studied. The hardness of the ceramics decreased with increasing TiB_2 content. Monolithic SiC had a Vickers hardness of 27.8 GPa while monolithic TiB_2 had a hardness of 24.4 GPa. In contrast, fracture toughness of the ceramics increased from 2.1 $MPa \cdot m^{1/2}$ for nominally pure SiC to ~6 $MPa \cdot m^{1/2}$ for SiC with TiB_2 contents of 40 vol.% or higher. Flexure strengths were measured for three composites SiC-15TiB_2, SiC-20TiB_2, and SiC-40TiB_2 and the results were analyzed using a two parameter Weibull analysis. The ceramic containing 20 vol.% TiB_2 was the strongest with an average strength of 522 MPa. The ceramic containing 40 vol.% TiB_2 was the weakest with an average strength of 423 MPa. As TiB_2 content increased, the Weibull modulus increased from 12 for a TiB_2 content of 15 vol.% to 17 for TiB_2 contents of 20 and 40 vol.%. Analysis of the microstructure revealed microcracking in the composites containing 20 and 40 vol.% TiB_2 which accounted for the increased Weibull modulus and decreased hardness. The ceramic containing 40 vol.% TiB_2 had the best combination of properties with a fracture toughness of 6.2 $MPa \cdot m^{1/2}$, hardness of 25.3 GPa, Weibull modulus of 17, and a strength of 423 MPa.

INTRODUCTION

Silicon carbide (SiC) is a strong, hard, and chemically inert ceramic used in several applications that involve extreme environments.[1-5] In armor applications, the high hardness of SiC, which is commonly reported to be in the range of 20 to 27 GPa, is advantageous for projectile defeat.[6,7] Like most ceramics, however, SiC is brittle due to its low fracture toughness (2 to 5 $MPa \cdot m^{1/2}$), whereas a high fracture toughness is advantageous for multi hit capability.[4,5,8,9] The fracture toughness of SiC based ceramics can be improved to as high as 6 to 9 $MPa \cdot m^{1/2}$ with additives that promote densification and crack propagation along the grain boundaries as well as increasing the grain size.[1,8,10] However, an increase in toughness is typically accompanied by a drop in hardness.[8,9,11-13] Flinders et al. reported a hardness of 20 GPa and a fracture toughness of 2.6 $MPa \cdot m^{1/2}$ for SiC with no sintering additives, but saw the hardness drop to 14 GPa while fracture toughness increased to 6.7 $MPa \cdot m^{1/2}$ for SiC with 3 wt.% aluminum sintering aids.[8] Titanium diboride (TiB_2) exhibits a high hardness (25-35 GPa) and may help combat the hardness/toughness tradeoff when added as a reinforcing phase in SiC.[14-17]

Studies on SiC-TiB_2 composites have mainly focused on the increase in toughness, which has been attributed to crack deflection and bridging effects due to the presence of TiB_2 particles.[17-21] SiC has a thermal expansion coefficient (CTE) along the c-direction of 4.45 x $10^{-6}/^{o}C$ and 3.67 x $10^{-6}/^{o}C$ along the a-direction. TiB_2, however, has a higher CTE in each direction: 8.6 x $10^{-6}/^{o}C$ along the c-direction and 6.6 x $10^{-6}/^{o}C$ along the a-direction.[14,22,23] This mismatch in CTE values puts the SiC matrix in compression and the TiB_2 particles in tension after cooling from the typical densification temperatures

(1900-2200^{o}C) in a SiC-TiB_2 ceramic composite.[17,24,25] The mismatch promotes toughening due to the thermal residual stresses and resulting crack deflection that can occur as cracks are drawn to the interface between the SiC matrix, which is in compression, and the TiB_2 particles where the highest tensile stresses exist.[26] Blanc showed an increase in toughness from 3.5 MPa·$m^{1/2}$ to 3.9 MPa·$m^{1/2}$ with a hardness decrease from 30 GPa to 23 GPa as TiB_2 content increased from 5 to 15 vol.%.[15] Bucevac, measuring toughness using the indentation method, saw a toughness boost from 4.3 MPa·$m^{1/2}$ to 5.3 MPa·$m^{1/2}$ as TiB_2 content increased from 12 to 24 vol.%; however hardness data was not presented.[27]

The purpose of this paper is to examine the properties of SiC-TiB_2 ceramic composites with TiB_2 contents ranging from 0 to 100 vol.%. Fracture toughness and hardness were measured for each composition. Based on their measured hardness and fracture toughness values, Young's modulus and flexure strength were measured for SiC-TiB_2 ceramics containing 15, 20, and 40 vol.% TiB_2. A two parameter Weibull analysis was used to analyze the behavior of SiC-TiB_2 ceramics tested in flexure.

EXPERIMENTAL PROCEDURE

SiC-TiB_2 ceramic composites with TiB_2 contents ranging from 0 to 100 vol.%, were batched using commercially available SiC (H.C. Starck; Grade UF-25; α-SiC; Newton, MA) and TiB_2 (Momentive; Grade HCT-F; Columbus, OH) powders. To promote densification, 1 wt% B_4C (H.C. Starck; Grade HS) and 2 wt.% C, in the form of phenolic resin (GP 2074, Georgia Pacific Chemicals, Atlanta, GA), were ball milled with

the SiC and TiB_2 powders in a polyethylene jar using TiB_2 milling media and acetone. For the nominally pure SiC specimen, the same procedure was used except that SiC media were used instead of TiB_2 media. Compositions were designated as SiC-"X"TiB_2 where "X" is the nominal volume percentage of TiB_2. Resulting slurries were dried by rotary evaporation to minimize segregation of the constituents. The SiC-TiB_2 powders were then ground and sieved to -60 mesh before hot-pressing.

Initial billets of each composition, nominally 2.5 cm in diameter, were densified by hot pressing in a graphite element furnace (Thermal Technologies, H20-3060, Santa Rosa, CA) using a graphite die. To minimize reaction between dies and billets, dies were lined with graphite paper (0.254 mm thick GTA, Leader Global Technologies, Deer Park, TX) that was coated with boron nitride spray (SP-108, Materion, Milwaukee, WI) before the powder was loaded. Die assemblies were heated under vacuum at a rate of 50^oC/min. Isothermal holds were employed at 1450°C and 1650^oC to facilitate removal of oxide contamination from the surfaces of the powder particles. At 1450^oC the isothermal hold time was 2 hours. The furnace was then held at 1650^oC until the chamber pressure returned to the nominal vacuum pressure of 27 Pa (200 mtorr). Above 1650°C, and up to the final densification temperature, the atmosphere was changed to flowing argon at a pressure of ~10^5 Pa (~1 atm) and a uniaxial pressure of 32 MPa was applied. The final densification temperature was 2100^oC for nominally pure SiC and TiB_2 billets, but 1980^oC for the intermediate compositions. Pressing ceased after ram travel had stopped for a period of ten minutes, and the furnace was allowed to cool to room temperature naturally. For compositions that were selected for flexure testing,

billets that were nominally 55 mm by 55 mm by 5mm were hot pressed in a graphite element furnace (Thermal Technologies Inc., Model HP50-7010G). Because of the larger die size, and increased powder volume, 50^{o}C was added to the isothermal hold temperatures, including the final densification temperature.

The bulk densities were measured for all billets using the Archimedes' method. The theoretical density for each composite was calculated based on the nominal volumetric ratios of SiC and TiB_2. The 55 mm by 55 mm by 5 mm billets were machined into mechanical test bars using an automated surface grinder (Chevalier Machinery Inc., Model FSG-3A818, Santa Fe Springs, CA) following the guidelines of ASTM C1161-02c for B-bars (3 mm by 4 mm by 45 mm). Specimens were tested in four point bending with a fully articulated fixture (20 mm upper span x 40 mm lower span), using a screw-driven load frame (Instron, Model 5881, Norwood, MA) that was computer controlled (Instron, Bluehill 2, Norwood, MA). For SiC-15TiB_2, 39 bars were tested to failure while 36 bars were tested for SiC-20TiB_2, and 38 for SiC-40TiB_2. All of the specimens from each composition were analyzed using a two parameter Weibull distribution, calculated from the failure stresses. Elastic constants were determined using the impulse excitation method (Grindosonic Mk5 Industrial, J.W. Lemmens Inc., Heverlee, Belgium) following ASTM C1259-08e1.

Vickers' hardness was measured (Struers Inc., Duramin 5, Cleveland, OH) using a load of 1 kg with a 15 s dwell time. Reported values were an average of 10 hardness indents. Hardness specimens were prepared by mounting sections of broken flexure bars

and cross-sectioned billets in an epoxy resin and polishing to a mirror finish using successively finer diamond abrasives to a 0.25 μm surface finish. Fracture toughness was determined using direct crack measurements. Specimens were indented (Leco Corporation, Model V-100-A2, St. Joseph, MI) with a load of 5 kg on a polished surface with a Vickers diamond tip followed by measurements of the radial median cracks formed during indentation.[28]

Polished specimens were examined using scanning electron microscopy (S-570, Hitachi, Tokyo, Japan and Helios Nanolab 600, FEI, Hillsboro, OR). Area fractions of the constituent phases and porosity were determined using computer image analysis (ImageJ, National Institutes of Health, Bethesda, MD). Particle size was determined by equating average particle area to the area of a sphere with equivalent diameter.

RESULTS AND DISCUSSION

Table I summarizes the density values for each SiC-TiB_2 ceramic. Theoretical densities were calculated based on the nominal SiC and TiB_2 contents without accounting for sintering aids (C and B_4C) since some of them were consumed by reaction with surface oxide impurities during hot pressing.[29-31] Because of the retention of some low density B_4C and/or C in the final ceramics, relative densities represent a lower bound for the relative density and likely underestimate the actual relative density. Likewise, pores can reduce the value of the measured bulk density of the ceramics. Even though the relative density values may underestimate actual density, all of the relative densities were

more than 97%, with most being 99%. Hence, hot-pressing proved to be effective for densifying all of the compositions.

Microstructures were analyzed for all of the hot pressed composites (Figure 1). The SEM images were consistent with the density measurements and supported the conclusion that the specimens contained a small volume fraction of porosity (<1%). Both residual sintering aids and porosity appear dark, but porosity could be identified as dark inclusions with a light ring around them due to beam charging. Charging can also be seen around grain pullout that occurred through the polishing procedure, but can be distinguished from porosity due to the jagged corners, whereas pores appear circular. While Figure 1f (nominally 100% TiB_2) appears to be porous, the composition was 97% dense (Table I). The residual B_4C or carbon sintering aids that are retained after sintering were apparent in the micrographs as dark regions without charging around them. In addition to porosity and sintering additives, the SEM images also showed that the SiC and TiB_2 were uniformly distributed. Average TiB_2 particle sizes were measured for each ceramic and were used in the interpretation of strength data. Based on equivalent circular diameters, the size of TiB_2 particles increased from 2.1 μm for SiC-15TiB_2 to 6.3 μm for SiC-20TiB_2 and to 26.2 μm for SiC-40TiB_2. The increase in particle size as TiB_2 content increased also led to an increase in the average distance between TiB_2 particles. As a result, a crack propagating through the microstructure must travel farther through the SiC matrix between TiB_2 inclusions in SiC-40TiB_2 than in SiC-20TiB_2 or SiC-15TiB_2. The longer path through SiC should increase the toughening in SiC-TiB_2 composites due to the presence of compressive thermal residual stresses in the SiC.[16,27]

The measured Vickers hardness values for SiC-TiB_2 ceramics decreased as TiB_2 content increased (Table I). In contrast, an increase in hardness is expected as TiB_2 content increases. Using reported hardness values of 27 GPa for SiC and 33 GPa for TiB_2, a volumetric rule of mixtures calculation can be used to estimate the increase in hardness with increasing TiB_2 content.[7,14,15,32] For the measured values, nominally pure SiC had the highest hardness at 28 GPa while SiC-80TiB_2 and TiB_2 had the lowest values at 24 GPa. The drop in the hardness with increasing TiB_2 content indicates a reduction in the work of indentation, which may be related to the distribution of areas with residual tensile stresses.[33,34] Microcracking, which can be caused by crystal anisotropy in nominally pure TiB_2, or by thermal residual stresses within SiC-TiB_2 composites, can also decrease measured hardness values because the work of indentation is decreased through the closing of microcracks.[14,32] In the SiC-TiB_2 ceramics, tensile stresses that develop during cooling due to the CTE mismatch between SiC and TiB_2 may lead to microcracking, which could have led to the decrease in hardness when an increase was expected.

Fracture toughness measurements are also summarized in Table I. With increasing additions of TiB_2, fracture toughness increased from 2 $MPa \cdot m^{1/2}$ for nominally pure SiC to 6.2 $MPa \cdot m^{1/2}$ for SiC-40TiB_2. The toughness values plateaued at ~6 $MPa \cdot m^{1/2}$ for SiC-TiB_2 ceramics with TiB_2 contents above 40 vol.%. For compositions containing more than 40 vol.% TiB_2, the microstructures transition from isolated TiB_2 particles in a SiC matrix to isolated SiC particles in a TiB_2 matrix. The change in the number of SiC particles appeared to have no effect on the measured toughness since both

SiC-60TiB_2 and SiC-80TiB_2 have the same nominal fracture toughness as nominally pure TiB_2 (~6 MPa·$m^{1/2}$). Whereas TiB_2 additions to SiC had a major effect on fracture toughness due to the residual compressive stresses generated in the SiC matrix, the addition of SiC to TiB_2 did not appear to affect the toughness compared to nominally pure TiB_2.

Figure 2 shows hardness and fracture toughness as a function of TiB_2 content. The classic hardness/toughness tradeoff is apparent in these materials as the hardness generally decreases across the composition range while the toughness increases.[9,11-13] Compared to SiC, a decrease of 9% in hardness was observed as TiB_2 content increased from 0 to 40 vol.% while toughness increased by >195% for SiC-40TiB_2 versus SiC. With both hardness and toughness being key properties for armor applications, SiC-40TiB_2 appeared to have the best combination of hardness and fracture toughness of the compositions tested, with a hardness of 25 GPa and fracture toughness of 6.2 MPa·$m^{1/2}$.[9,11,12,35]

The magnitude of thermal residual stresses, and the toughening due to compressive stresses within the matrix, were calculated over the range from processing temperature (2030^{o}C) to room temperature (25^{o}C) using the method outlined by Taya et al.[16] As the volume of TiB_2 increased, the magnitude of the tensile thermal residual stresses in the TiB_2 particles decreased from 1975 MPa in SiC-15TiB_2 to 1389 MPa in SiC-40TiB_2. Over the same composition range, the compressive stress in SiC increased from -349 MPa to -926 MPa. As the TiB_2 content increases, the residual compressive

stresses are distributed over a smaller volume fraction of SiC. As TiB_2 transitions from isolated particles to the matrix phase, the compressive stresses continue to build to ~1.5 GPa within the SiC particulate phase of SiC-80TiB_2. Based on the magnitude of these stresses, the amount of toughening due to compressive thermal residual stresses can be calculated. Conversely, a decrease in toughening due to tensile thermal residual stress can also be calculated using this method. This change in toughening, ΔK_I, was calculated for composites containing 15, 20, and 40 vol.% TiB_2. The amount of toughening was -0.58 $MPa \cdot m^{1/2}$ for SiC-15TiB_2, -1.16 $MPa \cdot m^{1/2}$ for SiC-20TiB_2, and -2.32 $MPa \cdot m^{1/2}$ for SiC-40TiB_2. These calculated ΔK_I's are equivalent to an increase in the toughening of the ceramic composites, ΔK_R.[16] Since TiB_2 pins grain growth of the SiC matrix during densification, a fine grained SiC matrix is produced. As a result, a fracture toughness of 2 $MPa \cdot m^{1/2}$ was used as a baseline value for the matrix, based on the reported fracture toughness for SiC with an average grain size of ~110 nm.[5] Based on thermal residual toughening the composite toughness should be 2.6 $MPa \cdot m^{1/2}$ for SiC-15TiB_2, 3.2 $MPa \cdot m^{1/2}$ for SiC-20TiB_2, and 4.3 $MPa \cdot m^{1/2}$ for SiC-40TiB_2. However, the expected increase in toughness for SiC, due to thermal residual stresses and compared to the baseline, value falls short of the measured K_{IC} values for all of the compositions. In other words, additional ΔK_R from other sources is needed to explain the toughness values measured for each ceramic composite. In a similar system (ZrB_2-SiC), Watts et al. showed using neutron diffraction that this temperature range may not be the optimum range as stresses between two different phases may start to accumulate at temperatures below the processing temperature (~1400^oC for ZrB_2-SiC).[36,37] Because of this, the

calculated thermal residual stress may be lower than calculated and the calculated ΔK_R may also not be as large as expected.

Crack deflection around particles is another possible toughening mechanism in ceramic composites. In many SiC-TiB_2 composites, crack deflection is thought to be the main mechanism of toughening.[17,19-21,24] Indeed, as a crack propagates through a SiC matrix that is in compression, the radial tensile stresses in the TiB_2 particles draws the crack(s) to these regions of the microstructure, which reduces the driving force for crack propagation in the tensile regions.[26] In the present study, crack deflections were observed near TiB_2 grains (Figure 3) by examining the paths of the radial/median cracks produced by indentations used in the determination of fracture toughness. For SiC-15TiB_2, a total of 53 deflections were counted in the four radial/median cracks produced by a 5 kg indent in a previous study.[38] The presence of crack deflection shows that in SiC-TiB_2 ceramics more than one toughening mechanism enhances fracture toughness.

The strongest SiC-TiB_2 composition tested in flexure was SiC-20TiB_2, with an average strength of 522 MPa. The next highest strength was 500 MPa for SiC-15TiB_2 followed by 423 MPa for SiC-40 TiB_2. The characteristic strengths were determined from the Weibull analysis. The characteristic strength is the value at which the probability of survival is 37%. The characteristic strengths follow the same pattern as the average strengths with the highest characteristic strength of 539 MPa for SiC-20TiB_2, the middle strength of 520 MPa for SiC-15TiB_2, and the lowest strength of 436 MPa for SiC-40TiB_2. The increasing matrix compressive stress due to the CTE mismatch between

TiB_2 and SiC seems to increase the strengths of SiC-15TiB_2 and SiC-20TiB_2 compared to nominally pure SiC. However, the trend did not follow for higher TiB_2 contents. For SiC-40TiB_2, the compressive stresses in the SiC matrix (-926 MPa) did not correlate to higher average strength. In this case, the lower strength indicates a larger flaw size in SiC-40TiB_2, which may indicate the presence of microcracking.[26]

Flexure strengths were analyzed using a two parameter Weibull analysis. Figure 4 shows the Weibull plot for each SiC-TiB_2 composition that underwent flexure testing. As TiB_2 content increased, so did the Weibull modulus. A Weibull modulus of 12 was calculated for SiC-15TiB_2, which increased to 17 for SiC-20TiB_2 and SiC-40TiB_2. Unlike the strengths, the TiB_2 content did not have a detrimental effect on the Weibull modulus. The higher Weibull modulus of SiC-20TiB_2 and SiC-40TiB_2 indicates that both of these SiC-TiB_2 ceramics have a smaller critical flaw size distribution than SiC-15TiB_2.

Young's modulus measurements using the dynamic impulse method were made on each composition that underwent Weibull analysis. Using Young's modulus values of 450 GPa for SiC and 560 GPa for TiB_2, a volumetric rule of mixtures calculation was also used to predict modulus values for the different compositions..[14,39] A measured value of 464±4 GPa for SiC-15TiB_2 agreed well with the predicted value of 467 GPa. In contrast, measured values of 454±5 GPa for SiC-20TiB_2 and 482±1 GPa for SiC-40TiB_2 fell below their predicted values of 472 GPa and 494 GPa. Based on the strength trends, thermal residual stresses seem to boost the strength of SiC-20TiB_2 due to the higher

compressive stresses in the SiC matrix compared to SiC-15TiB_2; however, thermal residual stresses may have been high enough in SiC-40TiB_2 to initiate microcracking, which gave that composition the lowest strength. Since porosity was minimal in all of the compositions, the decreases in Young's moduli support the conclusion of microcracking in SiC-40TiB_2 and SiC-20TiB_2.

Since many of the differences between measured values of mechanical properties and the expected values could be explained by microcracking, the particle size needed for spontaneous microcracking was calculated for each of the compositions examined using Weibull analysis.[40] The critical TiB_2 particle size was calculated to be ~10 μm for SiC-15TiB_2 and SiC-20TiB_2. In SiC-40TiB_2, a higher fracture toughness led to an increase in the critical TiB_2 particle size for spontaneous microcracking, which was calculated to be ~21 μm. While the average particle size of TiB_2 in SiC-15TiB_2 and SiC-15TiB_2 was below the calculated threshold for spontaneous microcracking, the maximum particle sizes measured were 14.3 μm and 23.0 μm, respectively. However, in SiC-15TiB_2 particle sizes over 10 μm occurred at a frequency of 0.3% compared to 9% of TiB_2 particles in SiC-20TiB_2 that were over the threshold. Because of the low percentage of particles above the threshold in SiC-15TiB_2, if microcracks existed, they would not be expected to affect the properties of the ceramic. This is similar to how small amounts of porosity are often assumed to have a negligible effect.[26,41] In SiC-20TiB_2, however, the drop in hardness and Young's modulus are consistent with the presence of microcracking. In SiC-40TiB_2, TiB_2 particle size is above the calculated limit. To complement the calculations, high resolution SEM images (Figures 5 and 6) show what

appear to be circumferential microcracks at the interface between the TiB_2 particles and the SiC matrix grains in both SiC-20TiB_2 and SiC-40TiB_2.

Even though crack deflection was prevalent in each SiC-TiB_2 composites, microcracking can also lead to a rise in toughening as has been reported for SiC-TiB_2 ceramics.[42-44] Circumferential microcracking leads to an increase in toughness by shielding the tip of a propagating crack.[40,42,45] As circumferential microcracking is seen in both SiC-20TiB_2 and SiC-40TiB_2, but not SiC-15TiB_2, microcracking appears to have a major effect on increasing the fracture toughness of SiC-TiB_2 composites compared to toughening through thermal residual stresses and crack deflection.

In SiC-20TiB_2 and SiC-40TiB_2, microcracking is the likely cause of the higher Weibull moduli compared to the non-microcracked SiC-15TiB_2. Since both ceramics had TiB_2 particle sizes large enough to expect spontaneous microcracking, stress induced microcracking would also be expected during flexure testing.[46] In ceramics, a microcracked process zone due to stress induced microcracking can lead to crack tip shielding, allowing the material to exhibit R-curve behavior.[42,45,47] R-curve behavior was not tested in the present study, but increasing R-curve behavior has been reported to accompany an increase in Weibull modulus in previous studies.[42,48-50] While microcracks were observed in SiC-20TiB_2 (Fig. 5), they appeared to have no effect on the strength of the ceramic as the strength of SiC-20TiB_2 was higher than SiC-15TiB_2. However, microcracking can increase the flaw size, which reduces the strength, as seen in SiC-40TiB_2. Therefore, the measured strength of SiC-20TiB_2 may be lower than a SiC-20TiB_2

ceramic without microcracking.[26,51] Similarly, in a previous study, SiC-15TiB_2 was compared to a ceramic produced using commercially available SiC-TiB_2 spray dried granules with 15 vol.% TiB_2. While SiC-15TiB_2 did not exhibit microcracking, the ceramic produced from commercially available spray dried granules exhibited microcracking and suffered a drop in strength compared to SiC-15TiB_2.[38] Compared to the other SiC-TiB_2 composites, an increased fracture toughness (6.2 MPa·$m^{1/2}$), high hardness (25.3 GPa) and a high Weibull modulus (17) make SiC-40TiB_2 a good candidate for ceramic armor consideration.

CONCLUSIONS

The mechanical properties were studied for SiC-TiB_2 ceramics as a function of TiB_2 content. The hardness decreased almost linearly from 27 GPa for nominally pure SiC to 24 GPa for nominally pure TiB_2. Fracture toughness increased from 2 MPa·$m^{1/2}$ for nominally pure SiC to a value of ~6 MPa·$m^{1/2}$ for TiB_2 contents of 40 vol.% and higher. Weibull analysis was used to evaluate the strength of three compositions, SiC-15TiB_2, SiC-20TiB_2, and SiC-40TiB_2. SiC-20TiB_2 had the highest flexural strength at 522 MPa followed by SiC-15TiB_2 at 500 MPa and SiC-40TiB_2 at 423 MPa. The lower strength of SiC-40TiB_2 combined with a lower-than-expected hardness value of 25 GPa suggested that microcracks were present in SiC-40TiB_2. Young's modulus measurements also suggested that microcracks existed in both SiC-20TiB_2 and SiC-40TiB_2. The measured Young's modulus value for SiC-15TiB_2, was 464 GPa, which agreed well with a predicted value of 467 GPa using the nominal composition and modulus values for nominally pure SiC and TiB_2. In contrast, the Young's modulus

values measured for SiC-20TiB_2 (454 GPa) and SiC-40TiB_2 (482 GPa) were below the predicted values of 472 GPa and 494 GPa, further indicating that microcracks may be present in these compositions. Threshold particle sizes for spontaneous microcracking were calculated to be ~10 μm in SiC-15TiB_2 and SiC-20TiB_2 and ~21 μm in SiC-40TiB_2. Analysis by SEM revealed that TiB_2 particle size increased from 2.1 μm in SiC-15TiB_2 and 6.3 μm in SiC-20TiB_2 to 26.2 μm in SiC-40TiB_2. While both SiC-15TiB_2 and SiC-20TiB_2 had average particle sizes under the spontaneous microcracking threshold, 10% of the measured particles in SiC-20TiB_2 were above the 10 μm mark and microcracking may not have had the same effect on the strength of SiC-40TiB_2. High resolution SEM was used to find evidence of the presence of circumferential microcracks at the interface between the TiB_2 particles and the SiC matrix grains in SiC-20TiB_2 and SiC-40TiB_2. Microcracking also helped boost the Weibull modulus of SiC-20TiB_2 and SiC-40TiB_2 to 17 compared to a value of 12 for SiC-15TiB_2, which did not have any microcracks. While it was the weakest, SiC-40TiB_2 exhibited high fracture toughness (6.2 $MPa \cdot m^{1/2}$), high hardness (25.3 GPa) and a high Weibull modulus making it a good candidate for ceramic armor consideration.

ACKNOWLEDGEMENTS

Research was sponsored by Saint-Gobain Ceramics and the Army Research Laboratory and was accomplished under Cooperative Agreement Number W911NF-08-2-0001. The views and conclusions contained in this document are those of the authors and should not be interpreted as representing the official policies, either expressed or

REFERENCES

[1]J. J. Cao, W. J. MoberlyChan, L. C. De Jonghe, C. J. Gilbert, and R. O. Ritchie, "In Situ Toughened Silicon Carbide with Al-B-C Additions," *J. Am. Ceram. Soc.*, **79**[2] 461-69 (1996).

[2]H. Endo, M. Ueki, and H. Kubo, "Hot pressing of SiC-TiC composites," *J. Mater. Sci.*, **25**[5] 2503-06 (1990).

[3]X. F. Zhang, M. E. Sixta, and L. C. D. Jonghe, "Grain Boundary Evolution in Hot-Pressed ABC-SiC," *J. Am. Ceram. Soc.*, **83**[11] 2813-20 (2000).

[4]M. Miura, T. Yogo, and S. I. Hirano, "Phase separation and toughening of SiC-AIN solid-solution ceramics," *J. Mater. Sci.*, **28**[14] 3859-65 (1993).

[5]Y.-W. Kim, M. Mitomo, and H. Hirotsuru, "Grain Growth and Fracture Toughness of Fine-Grained Silicon Carbide Ceramics," *J. Am. Ceram. Soc.*, **78**[11] 3145-48 (1995).

[6]B. Matchen, "Applications of Ceramics in Armor Products," *Key Eng. Mater.*, **122-124** 333-44 (1996).

[7]"Engineered Materials Handbook: Ceramics and Glasses," **Vol. 4**. ASM International, (1991).

[8]M. Flinders, D. Ray, A. Anderson, and R. A. Cutler, "High-Toughness Silicon Carbide as Armor," *J. Am. Ceram. Soc.*, **88**[8] 2217-26 (2005).

[9]P. G. Karandikar, G. Evans, S. Wong, M. K. Aghajanian, and M. Sennett, "A Review of Ceramics for Armor Applications," pp. 163-75. in Advances in Ceramic Armor IV: Ceramic Engineering and Science Proceedings, Volume 29, Issue 6**.** John Wiley & Sons, Inc., 2009.

[10]G. E. Hilmas and T.-Y. Tien, "Effect of AlN and Al_2O_3 additions on the phase relationships and morphology of SiC Part I Compositions and properties," *J. Mater. Sci.*, **34**[22] 5605-12 (1999).

[11]D. Ray, M. Flinders, A. Anderson, and R. A. Cutler, "Hardness/Toughness Relationship for SiC Armor," pp. 401-10. in 27th Annual Cocoa Beach Conference on Advanced Ceramics and Composites: A: Ceramic Engineering and Science Proceedings**.** John Wiley & Sons, Inc., 2008.

[12]D. Ray, M. Flinders, A. Anderson, R. A. Cutler, and W. Rafaniello, "Effect of Room-Temperature Hardness and Toughness on the Ballistic Performance of SiC-Based Ceramics," in International Conference on Advanced Ceramics and Composites. **Vol. 26**, *Advances in Ceramic Armor* Edited by J. J. Swab.

[13]S. J. Park, K. Cowan, J. L. Johnson, and R. M. German, "Grain size measurement methods and models for nanograined WC–Co," *International Journal of Refractory Metals and Hard Materials*, **26**[3] 152-63 (2008).

[14]B. Basu, "Processing and Properties of Monolithic TiB_2 Based Materials," *Int. Mater. Rev.*, **51**[6] 352-74 (2006).

[15]C. Blanc, F. Thevenot, and D. Goeuriot, "Microstructural and mechanical characterization of SiC-submicron TiB_2 composites," *J. Eur. Ceram. Soc.*, **19**[5] 561-69 (1999).

[16]M. Taya, S. Hayashi, A. S. Kobayashi, and H. S. Yoon, "Toughening of a Particulate-Reinforced Ceramic-Matrix Composite by Thermal Residual Stress," *J. Am. Ceram. Soc.*, **73**[5] 1382-91 (1990).

[17]D.-H. Kuo and W. M. Kriven, "Mechanical behavior and microstructure of SiC and SiC/TiB_2 ceramics," *J. Eur. Ceram. Soc.*, **18**[1] 51-57 (1998).

[18]Y. Ohya, M. J. Hoffmann, and G. Petzow, "Sintering of in-Situ Synthesized SiC-TiB_2 Composites with Improved Fracture Toughness," *J. Am. Ceram. Soc.*, **75**[9] 2479-85 (1992).

[19]C. H. McMurtry, W. D. G. Boecker, S. G. Seshadri, J. S. Zanghi, and J. E. Garnier, "Microstrutcture and Material Properties of SiC-TiB_2 Composites," *Bull. Am. Ceram. Soc.*, **66**[21] 325-29 (1987).

[20]M. A. Janney, "Mechanical Properties and Oxidation Behavior of Hot-Pressed SiC-15vol%-TiB_2 Composite," *Bull. Am. Ceram. Soc.*, **66**[2] 322-24 (1987).

[21]J. D. Yoon and S. G. Kang, "Strengthing and toughening behaviour of SiC with additions of TiB_2," *J. Mater. Sci. Lett.*, **14** 1065-67 (1995).

[22]Z. Li and R. C. Bradt, "Thermal Expansion and Thermal Expansion Anisotropy of SiC Polytypes," *J. Am. Ceram. Soc.*, **70**[7] 445-48 (1987).

[23]M. K. Ferber, P. F. Becher, and C. B. Finch, "Effect of Microstructure on the Properties of TiB_2 Ceramics," *J. Am. Ceram. Soc.*, **66**[1] C-2-C-3 (1983).

[24]K.-S. Cho, H.-J. Choi, J.-G. Lee, and Y.-W. Kim, "In situ enhancement of toughness of SiC-TiB_2 composites," *J. Mater. Sci.*, **33**[1] 211-14 (1998).

[25]M.-J. Pan, P. A. Hoffman, D. J. Green, and J. R. Hellmann, "Elastic Properties and Microcracking Behavior of Particulate Titanium Diboride-Silicon Carbide Composites," *J. Am. Ceram. Soc.*, **80**[3] 692-98 (1997).

[26]J. B. Wachtman, W. R. Cannon, and M. J. Matthewson, "Mechanical Properties of Ceramics," 2nd ed. John Wiley & Sons, Inc.: Hoboken, NJ, (2009).

[27]D. Bucevac, S. Boskovic, B. Matovic, and V. Krstic, "Toughening of SiC matrix with in-situ created TiB_2 particles," *Ceram. Int.*, **36**[7] 2181-88 (2010).

[28]G. R. Anstis, P. Chantikul, B. R. Lawn, and D. B. Marshall, "A Critical Evaluation of Indentation Techniques for Measuring Fracture Toughness: I, Direct Crack Measurements," *J. Am. Ceram. Soc.*, **64**[9] 533-38 (1981).

[29]S. C. Zhang, G. E. Hilmas, and W. G. Fahrenholtz, "Pressureless Sintering of ZrB_2–SiC Ceramics," *J. Am. Ceram. Soc.*, **91**[1] 26-32 (2008).

[30]S. Zhu, W. G. Fahrenholtz, G. E. Hilmas, and S. C. Zhang, "Pressureless Sintering of Zirconium Diboride Using Boron Carbide and Carbon Additions," *J. Am. Ceram. Soc.*, **90**[11] 3660-63 (2007).

[31]S. Prochazka and R. M. Scanlan, "Effect of Boron and Carbon on Sintering of SiC," *J. Am. Ceram. Soc.*, **58**[1-2] 72-72 (1975).

[32]T. S. Srivatsan, G. Guruprasad, D. Black, R. Radhakrishnan, and T. S. Sudarshan, "Influence of TiB_2 content on microstructure and hardness of TiB_2–B_4C composite," *Powder Technol.*, **159**[3] 161-67 (2005).

[33]L. Wang, H. Bei, Y. F. Gao, Z. P. Lu, and T. G. Nieh, "Effect of residual stresses on the hardness of bulk metallic glasses," *Acta Mater.*, **59**[7] 2858-64 (2011).

[34]T. R. Simes, S. G. Mellor, and D. A. Hills, "A Note on the Influence of Residual Stress on Measured Hardness," *The Journal of Strain Analysis for Engineering Design*, **19**[2] 135-37 (1984).

[35]P. Lundberg and B. Lundberg, "Transition between interface defeat and penetration for tungsten projectiles and four silicon carbide materials," *Int. J. Impact Eng.*, **31**[7] 781-92 (2005).

[36]J. Watts, G. Hilmas, W. G. Fahrenholtz, D. Brown, and B. Clausen, "Measurement of thermal residual stresses in ZrB_2–SiC composites," *J. Eur. Ceram. Soc.*, **31**[9] 1811-20 (2011).

[37]J. Watts, G. Hilmas, W. G. Fahrenholtz, D. Brown, and B. Clausen, "Stress measurements in ZrB_2–SiC composites using Raman spectroscopy and neutron diffraction," *J. Eur. Ceram. Soc.*, **30**[11] 2165-71 (2010).

[38]D. S. King, W. G. Fahrenholtz, and G. E. Hilmas, "Microstructural Effects on the Mechanical Properties of SiC-15vol.% TiB_2 Particulate Reinforced Ceramic Composites," *J. Am. Ceram. Soc.* (submitted June 2012).

[39]P. T. B. Shaffer and C. K. Jun, "The elastic modulus of dense polycrystalline silicon carbide," *Mater. Res. Bull.*, **7**[1] 63-69 (1972).

[40]D. J. Magley, R. A. Winholtz, and K. T. Faber, "Residual Stress in a Two-Phase Microcracking Ceramic," *J. Am. Ceram. Soc.*, **76**[3] 1641-44 (1990).

[41]A. Rezaie, W. G. Fahrenholtz, and G. E. Hilmas, "Effect of hot pressing time and temperature on the microstructure and mechanical properties of ZrB_2–SiC," *J. Mater. Sci.*, **42**[8] 2735-44 (2007).

[42]W. H. Gu, K. T. Faber, and R. W. Steinbrech, "Microcracking and R-curve behavior in SiC-TiB_2 composites," *Acta Metall. Mater.*, **40**[11] 3121-28 (1992).

[43]W. H. Gu and K. T. Faber, "Tensile Behavior of Microcracking SiC-TiB_2 Composites," *J. Am. Ceram. Soc.*, **78**[6] 1507-12 (1995).

[44]H. Cai, W. H. Gu, and K. T. Faber, "Microcrack Toughening in a SiC-TiB_2 Composite," in Proceedings of the American Society for Composites Fifth Technical Conference; composite materials in transition.

[45]R. O. Ritchie, "Mechanisms of fatigue crack propagation in metals, ceramics and composites: Role of crack tip shielding," *Mater. Sci. Eng., A*, **103**[1] 15-28 (1988).

[46]D. J. Green, "Stress-Induced Microcracking at Second-Phase Inclusions," *J. Am. Ceram. Soc.*, **64**[3] 138-41 (1981).

[47]G. D. Bowling, K. T. Faber, and R. G. Hoagland, "Computer Simulations of R-Curve Behavior in Microcracking Materials," *J. Am. Ceram. Soc.*, **70**[11] 849-54 (1987).

[48]J. Gong, W. Si, and Z. Guan, "Weibull modulus of fracture strength of toughened ceramics subjected to small-scale contacts," *J. Mater. Sci.*, **36**[10] 2391-96 (2001).

[49]S. Kaur, D. K. Shetty, and R. A. Cutler, "R Curves and Crack-Stability Map: Application to Ce-TZP/Al_2O_3," *J. Am. Ceram. Soc.*, **90**[11] 3554-58 (2007).

[50]D. K. Shetty and J.-S. Wang, "Crack Stability and Strength Distribution of Ceramics That Exhibit Rising Crack-Growth-Resistance (R-Curve) Behavior," *J. Am. Ceram. Soc.*, **72**[7] 1158-62 (1989).

[51]D. J. Green, "Critical Microstructures for Microcracking in Al_2O_3-ZrO_2 Composites," *J. Am. Ceram. Soc.*, **65**[12] 610-14 (1982).

Table I: Density, Hardness, and Fracture Toughness of SiC-TiB_2 Ceramics

Composition	Densification Temperature (^oC)	Theoretical Density (g/cm^3)	Bulk Density (g/cm^3)	Relative Density (%)	Hardness (GPa)	Fracture Toughness ($MPa \cdot m^{1/2}$)
SiC	2100	3.22	3.20	99	27.8±1.1	2.1±0.1
SiC-15TiB_2	2030	3.42	3.37	99	26.0±1.8	4.3±0.4
SiC-20TiB_2	2030	3.48	3.37	97	25.9±1.8	4.5±0.4
SiC-25TiB_2	1980	3.55	3.50	99	27.2±1.5	4.2±0.2
SiC-30TiB_2	1980	3.61	3.56	99	26.6±1.3	4.4±0.3
SiC-35TiB_2	1980	3.68	3.59	98	25.5±1.3	4.7±0.5
SiC-40TiB_2	2030	3.74	3.64	97	25.3±1.4	6.2±1.0
SiC-60TiB_2	1980	4.00	3.90	98	25.3±0.9	6.1±0.6
SiC-80TiB_2	1980	4.26	4.15	97	24.2±2.0	5.7±0.7
TiB_2	2100	4.52	4.39	97	24.4±1.7	5.9±1.0

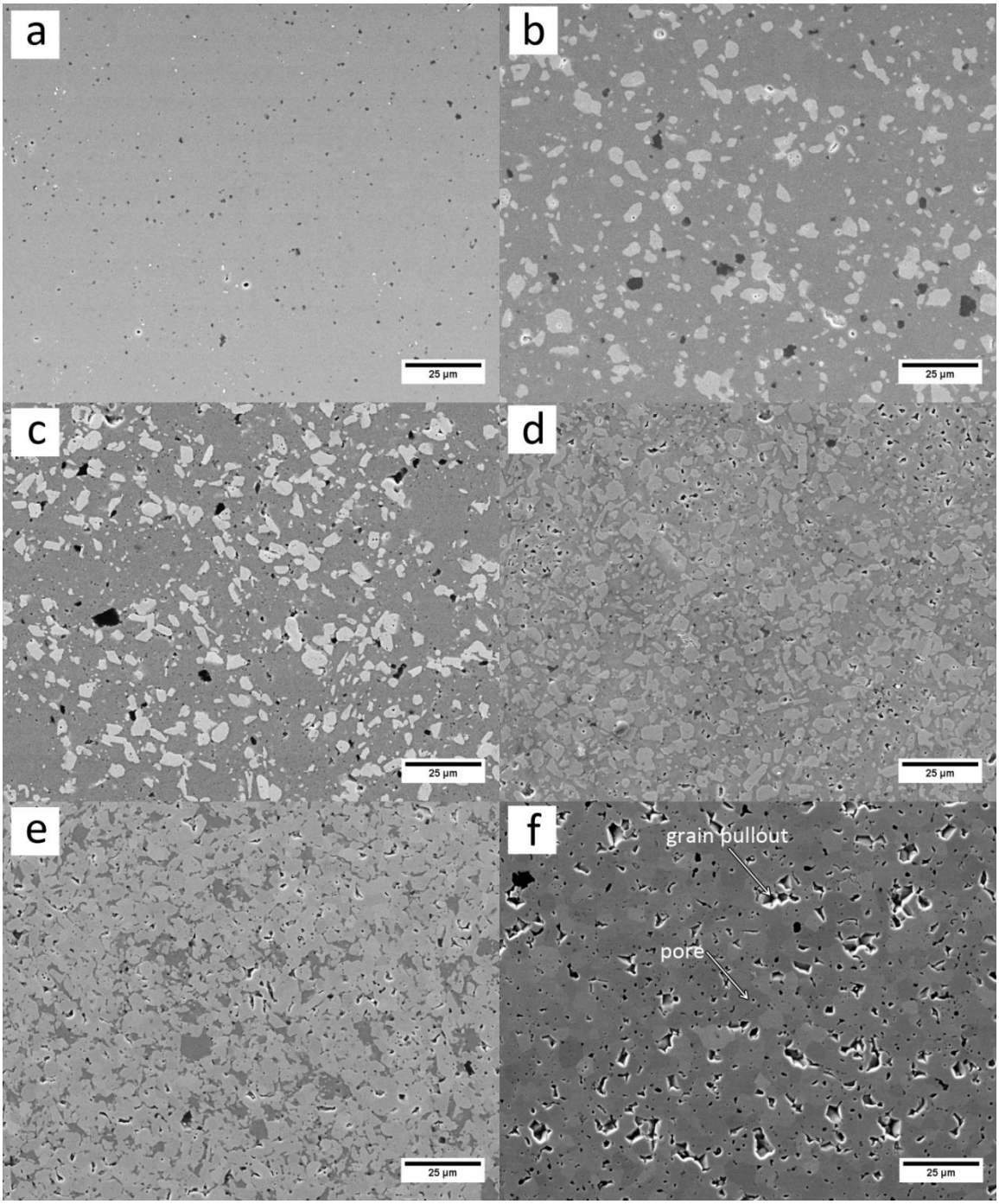

Fig. 1. SEM images of SiC (a), SiC-15TiB_2 (b), SiC-20TiB_2 (c), SiC-40TiB_2 (d), SiC-80TiB_2 (e), and TiB_2 (f). Compositions a-e appear to be dense, while still containing minimal porosity. Grain pullout in (f), however, makes the composition appear as if it is not dense. Arrows point to examples of grain pullout and a pore.

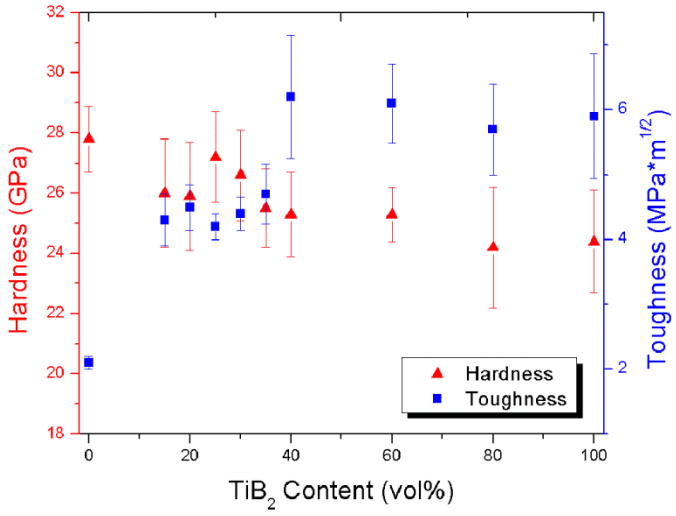

Fig. 2. Hardness and fracture toughness vs. TiB_2 content. Hardness decreases as TiB_2 content increases while fracture toughness increases.

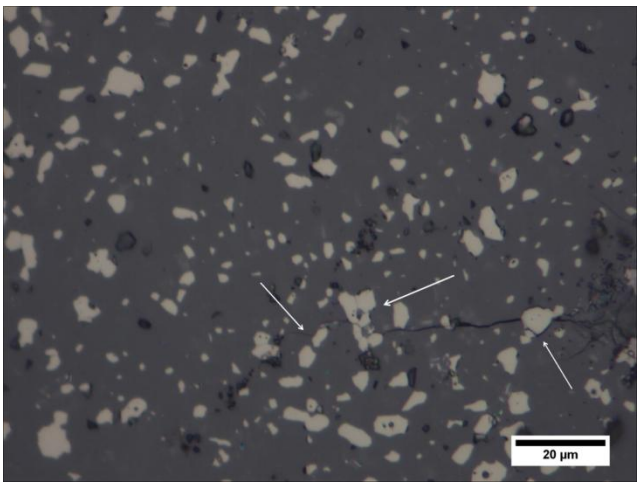

Fig. 3. Crack deflection at the corner of a Vickers indent in SiC-15TiB_2.

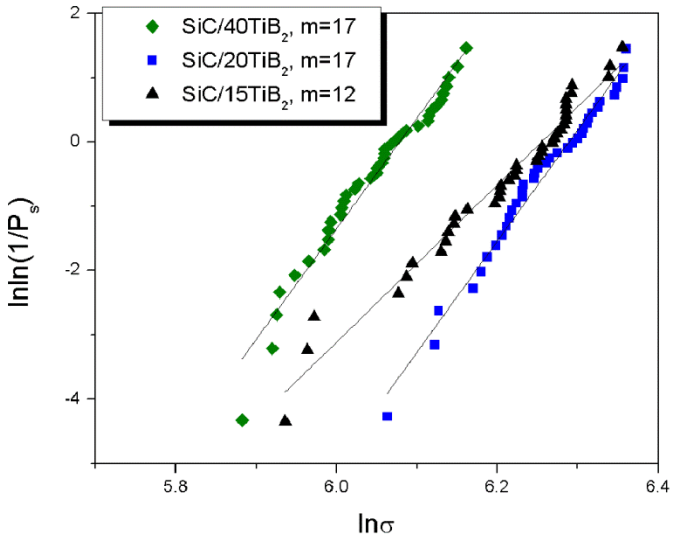

Fig. 4. Two-parameter Weibull analysis of SiC-TiB_2 compositions with 15, 20, and 40 vol.% TiB_2. Weibull modulus (m) increases as TiB_2 content increases.

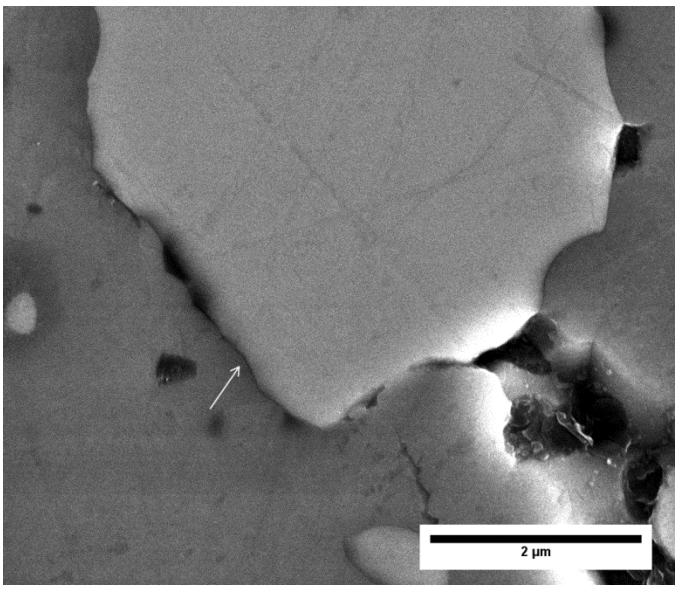

Fig. 5. SEM image of a circumferential microcrack around a TiB_2 grain in SiC-20TiB_2.

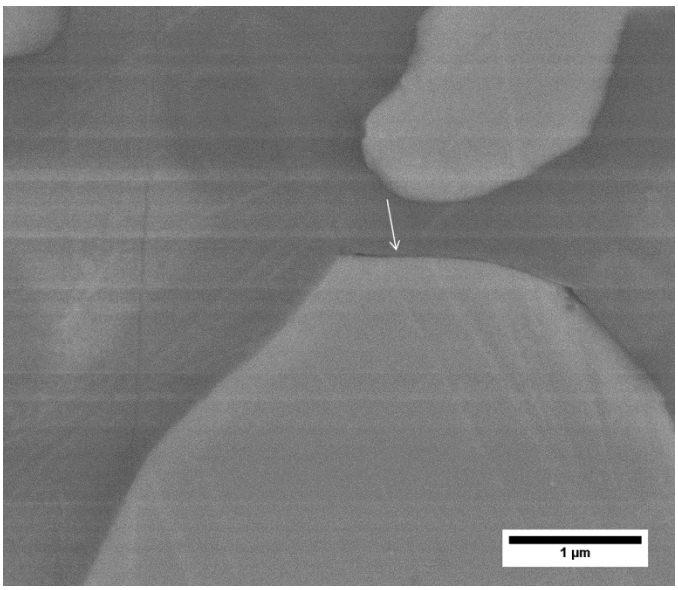

Fig. 6. SEM image of a circumferential microcrack around a TiB_2 grain in SiC-40TiB_2.

SECTION

3. SUMMARY AND CONCLUSIONS

3.1 SUMMARY OF RESULTS

The microstructure and mechanical properties of several silicon carbide-titanium diboride ceramic composites were studied. Two studies were presented in the form of manuscripts for submission to technical journals. The first paper compared the microstructure and mechanical properties of ceramics produced by hot pressing a commercially available SiC-TiB_2 powder (ST) to a SiC-TiB_2 (SiC-15TiB_2) ceramic prepared from SiC and TiB_2 powders along with sintering aids. The second paper focused on the effect that TiB_2 additions had on the microstructure and mechanical properties of SiC-TiB_2 ceramics. Whereas the first study focused on SiC containing 15 vol.% TiB_2, the second study examined SiC-TiB_2 ceramics with a range of TiB_2 contents. In this section, a summary from each paper is presented followed by some overall conclusions.

3.1.1 Paper I: Microstructural Effects on the Mechanical Properties of SiC-15vol.% TiB_2 Particulate Reinforced Ceramic Composites. Two SiC-TiB_2 ceramics containing nominally 15 vol.% TiB_2 were analyzed for their potential use in armor applications. Hot-pressing was used to densify both ceramics to >99% relative density. Microstructural analysis revealed that SiC-15TiB_2 exhibited a uniform microstructure while ST retained remnants of the starting granules where TiB_2 had segregated to the outside of the spray dried granules used to prepare the ceramics. Hardness, fracture toughness, strength, Young's modulus, and Weibull modulus were measured for both ceramics. While each ceramic exhibited the same hardness of 26 GPa, the fracture

toughness of SiC-15TiB_2 was 4.3 MPa·$m^{1/2}$ compared to 3.1 MPa·$m^{1/2}$ for ST. The SiC-15TiB_2 ceramic also had a higher average strength (500 MPa) than ST (380 MPa). A two parameter Weibull analysis of the strengths revealed that ST had the higher Weibull modulus, 21, while SiC-15TiB_2 had a Weibull modulus of 12. The measured Young's modulus of SiC-15TiB_2 (465 GPa) matched the predicted value of 467 GPa. In contrast, the Young's modulus of ST was lower than the predicted value at 433 GPa. Decreases in fracture toughness, strength, and Young's modulus indicated that microcracking may have been present in ST, which was confirmed by high resolution SEM analysis. While both ceramics contained nominally 15 vol.% TiB_2, microstructural differences (granule like microstructure and microcracking) between ST and SiC-15TiB_2 accounted for difference between the mechanical properties of the ceramics.

3.1.2 Paper II: Silicon Carbide-Titanium Diboride Ceramic Composites. SiC-TiB_2 ceramics were produced with compositions ranging from nominally pure SiC to nominally pure TiB_2 with eight intermediate compositions. Each composition was hot-pressed to > 97% relative density. Hardness decreased from 28 GPa for nominally pure SiC to 24 GPa for SiC-80TiB_2 and TiB_2. The measured fracture toughness, however, increased from 2 MPa·$m^{1/2}$ for nominally pure SiC to ~6 MPa·$m^{1/2}$ for SiC-TiB_2 ceramics with TiB_2 contents of 40 vol.% or higher. Strength, Weibull modulus, and Young's modulus were compared for SiC-15TiB_2, SiC-20TiB_2, and SiC-40TiB_2. SiC-20TiB_2 exhibited the highest average strength of 522 MPa followed by SiC-15TiB_2 (500 MPa) and SiC-40TiB_2 (423 MPa). SiC-20TiB_2 and SiC-40TiB_2 had the highest Weibull moduli at 17 compared to a Weibull modulus of 12 for SiC-15TiB_2. The Young's moduli of SiC-20TiB_2 (454 GPa) and SiC-40TiB_2 (482 GPa) were lower than their predicted values

(472 and 494 GPa) based on the properties of the nominally SiC and TiB_2, while the measured Young's modulus of SiC-15TiB_2 (465 GPa) matched well with its predicted value (467 GPa). Decreases in the Young's modulus and hardness combined with an increase in Weibull modulus suggested microcracking was present within the microstructures of SiC-20TiB_2 and SiC-40TiB_2. High resolution SEM analysis was used to provide evidence of microcracking in these microstructures. While it had the lowest average strength, SiC-40TiB_2 exhibited the best combination of hardness and toughness for potential use as a ceramic armor.

3.2 OVERALL CONCLUSIONS

The research presented in this thesis focused on determining how powder processing methods and TiB_2 additions changed the mechanical properties of SiC-TiB_2 ceramics. Research was also conducted to determine if a particular SiC-TiB_2 ceramic composition had a superior combination of mechanical properties. Some of the overall conclusions that can be drawn from the research are as follows:

- Hot-pressing was a reliable method to densify SiC-TiB_2 ceramics.
- SiC-TiB_2 ceramics produced by hot pressing ST granules retained their granule like remnants through densification and into the final microstructure due to TiB_2 segregation at the outside of ST granules.
- The granule remnants in ST led to a more uniform, albeit larger flaw size (~70 μm) which increased the Weibull modulus but reduced the strength of ST (380 MPa) compared to SiC-15TiB_2 (500 MPa).

- While the magnitude of the thermal residual stresses predicted for SiC-15TiB_2 and ST were the same, -350 MPa compressive stress in SiC and 1975 MPa tensile stress in TiB_2, large TiB_2 agglomerate sizes (>4.4 μm) in ST led to microcracking within the ST microstructure. However, evidence of microcracking was not seen in SiC-15TiB_2.
- Microcracking and the remnants of TiB_2-rich shells on spray dried granules in the final microstructure combined to boost the Weibull modulus of ST to 21 compared to 12 for SiC-15TiB_2, which had a uniform distribution of TiB_2 particles; however, strength was reduced for ST due to the larger average flaw size.
- Hardness decreased with TiB_2 additions to SiC. SiC had a measured Vickers hardness of 28 GPa that decreased to 24 GPa for SiC-80TiB_2 and TiB_2.
- The fracture toughness of SiC-TiB_2 ceramics was better than monolithic SiC (2 $MPa \cdot m^{1/2}$) and increased with increasing TiB_2 additions to a value of ~6 $MPa \cdot m^{1/2}$ for SiC-TiB_2 ceramics containing 40+ vol.% TiB_2.
- The Weibull modulus increased from 12 to 17 as TiB_2 additions increased from 15 vol.% to 20 and 40 vol.%.
- SiC-40TiB_2 exhibited the best combination of hardness (25 GPa), fracture toughness (6.2 $MPa.m^{1/2}$), and Weibull modulus (17) which makes it a good candidate for ceramic armor applications.

The presence of TiB_2 particles induced spontaneous microcracking in some SiC-TiB_2 ceramics. Microcracking was more likely in ceramics with larger TiB_2 particles or a higher volume fraction of TiB_2. Microcracking can help boost fracture toughness by

promoting crack deflection and crack tip shielding. However, spontaneous microcracking increases the size and number of flaws in the microstructure, resulting in decreases in the Young's modulus and average strength of the ceramics. Spontaneous microcracking can also reduce the measured hardness because part of the work of indentation is consumed through the closing of microcracks. Residual stresses within the material can also have deleterious effects on the hardness.

To produce a SiC-TiB_2 ceramic with improved properties compared to the compositions studied, spontaneous microcracking should be eliminated from the microstructure and residual stresses should be minimized. Thermal residual stresses will always exist due to a CTE mismatch between SiC and TiB_2; however, residual stresses due to crystal anisotropy can be reduced by reducing grain size. Producing ceramics with a TiB_2 particle size that is on the brink of microcracking, but just under the threshold for spontaneous microcracking, may be an advantage. If SiC-TiB_2 ceramic containing 10-20 vol.% TiB_2 reinforcing phase could be manufactured in such a way that TiB_2 particles, below the spontaneous microcracking threshold, surrounded larger SiC regions, a propagating crack would likely avoid the compressive residual stresses in the large SiC regions and propagate through the surrounding SiC-TiB_2 region in which the TiB_2 phase is in tension, drawing cracks to SiC-TiB_2 interfaces. This would increase the strength, hardness, and Young's modulus of the ceramics, but still allow for stress-induced microcracking to occur, which would increase the Weibull modulus by narrowing the flaw size distribution and increase fracture toughness by promoting crack deflection and crack tip shielding.

4. FUTURE WORK

Research presented in this thesis showed how the microstructure and mechanical properties of SiC-TiB_2 ceramics changed based on both the powder processing method and the amount of TiB_2 additions. Future work could help answer questions that still remain about why the properties of SiC-TiB_2 ceramics differ from values predicted based on the properties of nominally pure SiC and TiB_2. In addition, future work could also suggest processing methods that could be utilized by industry to produce these ceramics. The suggestions presented in this section strive to close the gap between laboratory investigations and industrial production methods.

Ceramic composites examined in this thesis were produced by hot-pressing. Pressureless sintering of the SiC-TiB_2 composites would make SiC-TiB_2 ceramics more attractive in an industry setting where pressureless sintering helps reduce processing costs. The densification kinetics differ between hot-pressing and pressureless sintering. The potential to change the microstructure through pressureless sintering could change the mechanical properties exhibited by sintered SiC-TiB_2 ceramics compared to the hot pressed materials examined in this study.

Powder processing was carried out by milling in a solvent; however, aqueous based processing could reduce costs and environmental concerns. In order to optimize aqueous based processing, research on the effectiveness of sintering aids would be needed due to the increased oxidation of the powders during milling. While the final ceramic is still a SiC-TiB_2 ceramic, the advantages of aqueous processing are cutting solvent storage, handling, and waste as well as the cost of the solvent compared to water, all of which could cut overall processing costs.

Silicon carbide can be densified using liquid phase sintering aids. While some work was performed as part of this thesis research to sinter SiC-20TiB_2 composites using aluminum as a sintering aid, pressureless densification of SiC-TiB_2 ceramic composites has not received much attention. Additions of aluminum, boron, and carbon help promote densification during pressureless sintering through the formation of a liquid phase. By utilizing liquid phase sintering techniques, reduction in sintering temperatures could be used to reduce industry costs. For SiC ceramics, a boost in fracture toughness is usually accompanied with a drop in hardness. Future work on this subject could focus on improved sintering techniques through liquid phase sintering and how liquid phase sintering additives affect the mechanical properties of SiC-TiB_2 ceramics.

A two parameter Weibull analysis was used analyze the strength data for SiC-15TiB_2, SiC-20TiB_2 and SiC-40TiB_2, but the matrix material was not analyzed. A Weibull analysis of nominally pure SiC would be advantageous to see how the reinforced composites compare to the monolithic material.

Calculations for the TiB_2 particle sizes that would produce spontaneous microcracking were performed. Using these calculations, ceramics fabricated with a range of TiB_2 particle sizes could be used to study the effect of microcracking on Weibull modulus a specific SiC-TiB_2 composition. A full analysis would then be available to compare each particulate composite "armor" (with and without microcracking) with the matrix (SiC), commonly used in armor, in terms of hardness, fracture toughness, strength, Young's modulus, and Weibull modulus.

APPENDIX

A.1 UNPUBLISHED DATA

A.1.1 Weibull Analysis of Polished SiC-20TiB_2. Table A.1 summarizes all of the properties obtained from the six ceramic composites tested in flexure for Weibull analysis. In an attempt to determine the critical flaw size more accurately, two sets of SiC-20TiB_2 flexure bars were polished to a 0.25 μm finish prior to flexure testing to reduce the flaw size compared to the standard surface finish of 600 grit. Results from this data are also included in Table A.1 as the first and second analysis. From Table I, the strengths of the polished bars were lower (~400 MPa) when compared to the 600 grit finish (~520 MPa). Weibull analysis of the data (Figure A.1) also shows a drop in Weibull modulus from 17 for 600 grit specimens to 7 for the polished specimens. Except for the two low strengths in the 1st analysis, the data for the 1st and 2nd analysis lie almost directly on top of each other, showing the consistency in production. However, in the 1st analysis there are two low strengths that skew the fit of the Weibull analysis and the Weibull modulus falls from 14 for the 2nd analysis to 7 for the first analysis. While they appear to be outliers in the data, these points cannot be disregarded since there is always a probability of having large flaws in brittle materials.[29]

Table A.1. Number of specimens tested in four-point flexure for Weibull analysis

Tested composite	Number of specimens (n)	Average Strength (MPa)	Characteristic Strength (MPa)	Weibull Modulus
Hexoloy ST	40	379±22	390	21
SiC-15TiB_2	39	499±48	520	12
SiC-20TiB_2	36	522±36	539	17
SiC-40TiB_2	38	423±30	436	17
0.25μm finish SiC-20 TiB_2, 1st analysis	35	401±58	430	7
0.25μm finish SiC-20 TiB_2, 2nd analysis	38	414±36	430	14

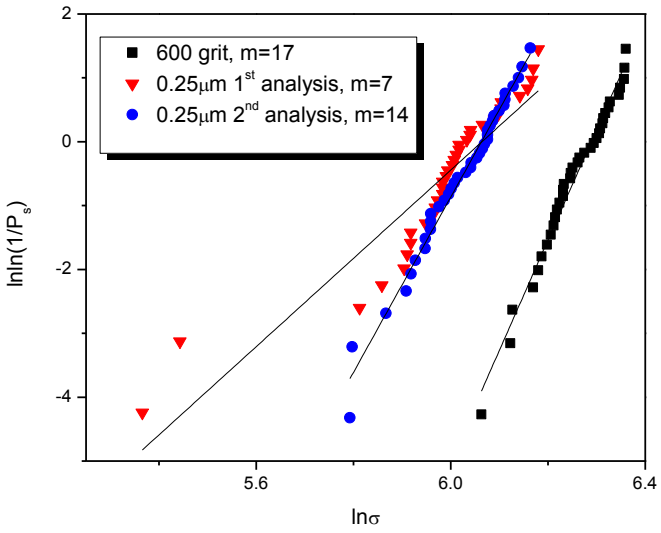

Figure A.1. Weibull distributions of SiC-20TiB_2 with a surface finishes of 600 grit and 0.25μm.

Figure A.2 contains SEM micrographs of the polished cross-sections of flexure bars that had a perpendicular face refinished using a 125μm polishing pad (2a) and a 15μm polishing pad (2b). The 125μm pad is typically used as a first pad to polish samples to a mirror finish by stepping down to successively smaller polishing grits. The 15μm pad was used to demonstrate a surface with a similar finish to a surface ground sample, since a 600 grit diamond grinding wheel for surface grinding of ceramics uses diamond grit between 13 and 16μm in size. From Figure A.2 it can be seen that the cross-section from the 125μm finish has sub-surface damage that has caused spalling along the edge of the cross-section and the finished surface. The depth of the sub-surface damage observed in Figure 7 (~20 to 35 μm) matches calculated critical flaw sizes, using Griffith theory, for both polished sets of Weibull data and can explain the observed decrease in strength for the flexure bars that underwent the diamond polishing operation.[29]

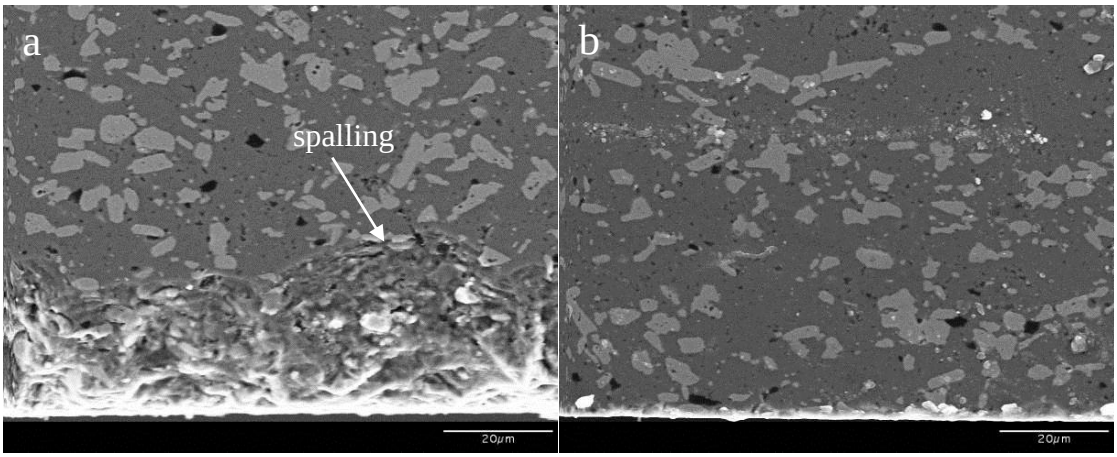

Figure A.2. Cross-section of ASTM C-1162 b-bar polished perpendicular to a (a)125μm surface finish and (b)15μm surface finish where the finished edged are at the bottom of the micrographs.

A.1.2 Pressureless Sintering of SiC-20TiB_2. Pressureless sintering of SiC-20TiB_2 with C and B_4C sintering aids was attempted using aqueous processing methods. Plyophen was used for a carbon source (supplied by St. Gobain). Powders were milled for 4 hours in water, using TiB_2 media. Two wt.% polyvinyl alcohol (523 polyvinyl alcohol, Airvol, Allentown, PA) was added as binder and milling continued for 24 hours. Powders were stir dried on a hot plate at ~100^oC for removal of water. Dried powders were and ground and sieved through a 60 mesh screen. Pellets nominally ½ in. in diameter were uniaxially pressed in a stainless steel die to a load of 1000 lbs. To increase green density, isostatic pressing (Fluitron Inc., CIP 6-24-30, Ivyland, PA) at a pressure of 30 ksi was also utilized. Binder burnout and phenolic char was performed in a burnout furnace (Lindberg, Type 51542-HR, Watertown, WI) under flowing argon (~1 atm). A ramp rate of 1^oC/min. was used with 2 hour isothermal holds at 400^oC and 800^oC. Sintering was performed in a graphite element furnace (Thermal Technologies Inc., Model 1000-4560 FP30), heated with a ramp rate of 10^oC/min. under vacuum (~200 mtorr) with 1 hour isothermal holds at 1450^oC and 1650^oC. The vacuum atmosphere was changed to flowing argon (~1 atm) and the furnace was ramped to 2150^oC at a rate of 15^oC/min. Due to sintering program errors, the pellets were only held at the final temperature (2150^oC) for ~6 min.. After cooling to room temperature the pellets appeared to contain a considerable amount of porosity. Optical microscopy of pellet cross-sections revealed that SiC-20TiB_2 melted and cooled through a eutectic (Figure 7.3). The eutectic melting temperature of SiC-TiB_2 has been measured to be 2190±40^oC for a SiC-TiB_2 volumetric ratio of 72:28.[84] At a ratio of 80:20, the phase diagram predicts the presence of SiC and a SiC-TiB_2 liquid above the eutectic temperature. Large

SiC grains in Figure A.3 indicate that eutectic melting is likely what occurred during sintering. Since pyrometers are used to measure temperatures above 600^{o}C in the furnace and since a pyrometer was used for determining the melting temperature of SiC-TiB_2 ceramics, difference in the pyrometer settings could change the accuracy of temperature measurement.

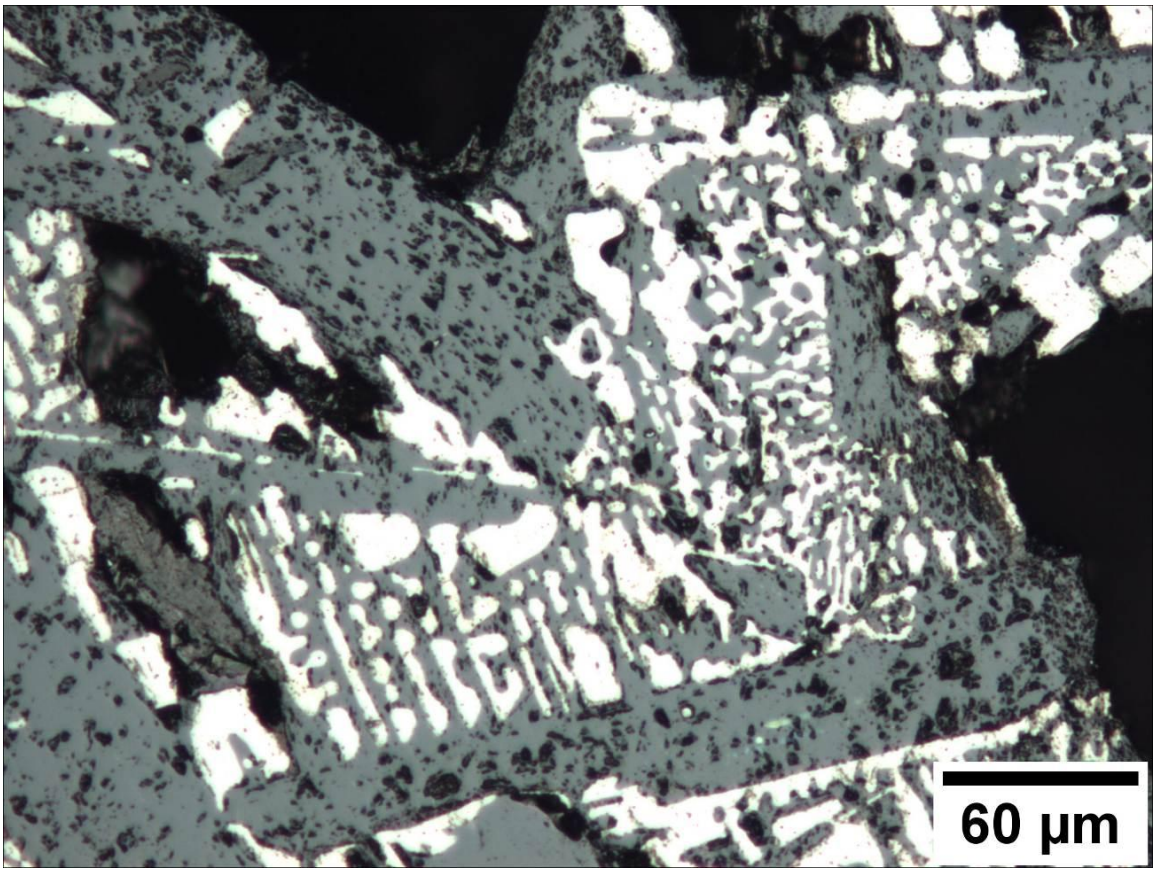

Figure A.3. SiC-20TiB_2 that underwent eutectic melting during pressureless sintering. Large SiC grains and a eutectic SiC-TiB_2 structure were observed.

A.1.3 Aluminum Additions to SiC-20TiB_2. An attempt was made at improving the mechanical properties of SiC-20TiB_2 by changing possible mechanisms of

densification. Aluminum, boron, and carbon (ABC) additions are sometimes added to SiC as sintering aids.[71,85,86] During sintering or hot-pressing a liquid phase with a composition similar to $Al_8B_4C_7$ forms which enhances densification. ABC SiC-TiB_2 powders were prepared and hot-pressed in the same manner as SiC-TiB_2 compositions pressed in the Thermal Technologies HP20-3060 furnace. Table A.2 includes the hardness and fracture toughness for a SiC-20TiB_2 composite densified with aluminum (3.5 wt%), B_4C (1 wt.%) and C (2 wt.%), referred to as ABC SiC-20TiB_2 to differentiate it from SiC-20TiB_2. With the ABC additions, the toughness was boosted from ~4.3 to ~4.8 MPa·$m^{1/2}$ without any weight gain as the theoretical densities of the two composites are nearly identical. The hardness of the ABC SiC-20TiB_2 composite, however, decreased by almost 4 GPa, 26 GPa (SiC-20TiB_2) to 22 GPa. This is a decrease of ~14% in hardness for the ABC composite compared to SiC-20TiB_2 with B_4C and C sintering aids.

Table A.2. SiC-20 TiB_2 vs. ABC SiC-20 TiB_2 (3.5wt% Al)

Material	***HV_1 (GPa)***	***Toughness ($MPa·m^{1/2}$)***	***Density (g/cm^3)***	***Relative density (%)***
SiC-20TiB_2	25.9±1.8	4.3±0.3	3.43	98.5
ABC SiC-20TiB_2	22.3±2.8	4.8±0.4	3.40	99.7

Pressureless sintering of ABC SiC-20TiB_2 was also attempted. Pellets were pressed using the same method used for SiC-20TiB_2 pellets. Pellets were sintered in a

graphite element furnace (Thermal Technologies Inc., 1000-3060 FP20). A ramp rate of 10^{o}C/min. under vacuum (~200 mtorr) was used with isothermal holds for oxide removal at 1450^{o}C for 20 min. and 1650^{o}C for 15 min. The vacuum atmosphere was replaced with flowing argon (~1 atm) after the 1650^{o}C isothermal hold and ramping continued at 5^{o}C/min. to a final densification temperature. Final densification temperatures of 1900, 1950, and 2000^{o}C were used. At 1950^{o}C for two hours, a maximum in bulk/relative density (3.26g/cm^{3}/96%) was achieved. Visually, without the aid of microscopes, rings appeared in the cross sections of ABC SiC-20TiB_2 pellets. EDS analysis in Figure A.4 of the pellets showed an aluminum depleted layer, ~325 μm deep, near the edge of the samples. Loss of aluminum may have occurred through reaction within the carbon crucible/furnace and the formation of aluminum carbide (Al_4C_8) which can become volatile at elevated temperatures.[87]

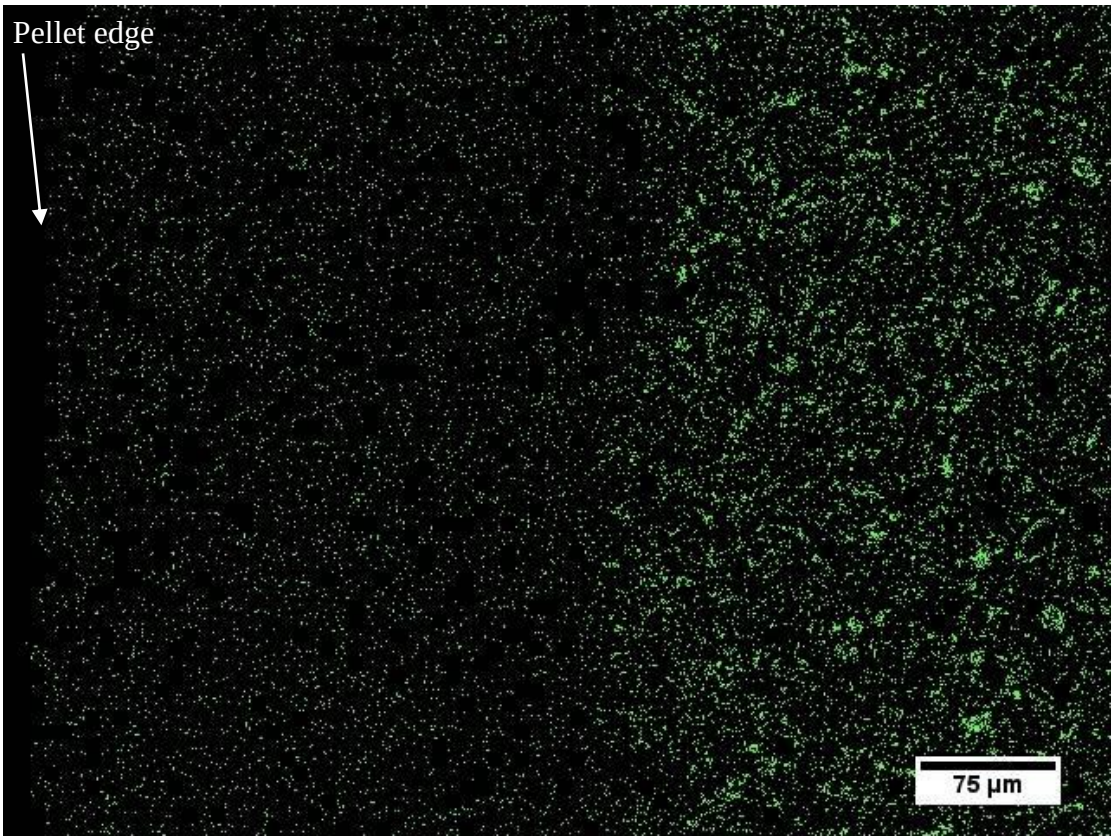

Figure A.4. EDS analysis of aluminum in ABC SiC-20TiB_2 showing that aluminum was depleted near the outer edge of the specimen.

REFERENCES

[1]K. Peleg, A. Rivkind, and L. Aharonson-Daniel, "Does Body Armor Protect from Firearm Injuries?," *Journal of the American College of Surgeons*, **202**[4] 643-48 (2006).

[2]N. Sekunda, "The Spartan Army." Osprey Publishing Limited, (1998).

[3]B. Dean, "Helmets and Body Armor of Modern Warfare," Yale University Press, (1920).

[4]National Institute of Justice (NIJ), "Ballistic Resistance of Body Armor", NIJ Standard 0101.062008, Washington, D.C.:National Institute of Justice.

[5]F. Thévenot, "Boron carbide—A comprehensive review," *J. Eur. Ceram. Soc.*, **6**[4] 205-25 (1990).

[6]P. G. Karandikar, G. Evans, S. Wong, M. K. Aghajanian, and M. Sennett, "A Review of Ceramics for Armor Applications," pp. 163-75. in Advances in Ceramic Armor IV: Ceramic Engineering and Science Proceedings, Volume 29, Issue 6**.** John Wiley & Sons, Inc., 2009.

[7]D. Ray, M. Flinders, A. Anderson, and R. A. Cutler, "Hardness/Toughness Relationship for SiC Armor," pp. 401-10. in 27th Annual Cocoa Beach Conference on Advanced Ceramics and Composites: A: Ceramic Engineering and Science Proceedings**.** John Wiley & Sons, Inc., 2008.

[8]M. Flinders, D. Ray, A. Anderson, and R. A. Cutler, "High-Toughness Silicon Carbide as Armor," *J. Am. Ceram. Soc.*, **88**[8] 2217-26 (2005).

[9]B. Basu, "Processing and Properties of Monolithic TiB_2 Based Materials," *Int. Mater. Rev.*, **51**[6] 352-74 (2006).

[10]J. C. LaSalvia, E. J. Horwath, E. J. Rapacki, C. J. Shih, and M. A. Meyers, "Microstructural and micromechanical aspects of ceramic/long-rod projectile interactions: dwell/penetration transitions," in Explomet. (2000).

[11]W. G. Fahrenholtz, E. W. Neuman, H. J. Brown-Shaklee, and G. E. Hilmas, "Superhard Boride–Carbide Particulate Composites," *J. Am. Ceram. Soc.*, **93**[11] 3580-83 (2010).

[12]"Engineered Materials Handbook: Ceramics and Glasses," **Vol. 4**. ASM International, (1991).

[13]Y.-W. Kim, M. Mitomo, and H. Hirotsuru, "Grain Growth and Fracture Toughness of Fine-Grained Silicon Carbide Ceramics," *J. Am. Ceram. Soc.,* **78**[11] 3145-48 (1995).

[14]G. E. Hilmas and T.-Y. Tien, "Effect of AlN and Al_2O_3 additions on the phase relationships and morphology of SiC Part I Compositions and properties," *J. Mater. Sci.,* **34**[22] 5605-12 (1999).

[15]C. Blanc, F. Thevenot, and D. Goeuriot, "Microstructural and mechanical characterization of SiC-submicron TiB_2 composites," *J. Eur. Ceram. Soc.,* **19**[5] 561-69 (1999).

[16]D. Bucevac, S. Boskovic, B. Matovic, and V. Krstic, "Toughening of SiC matrix with in-situ created TiB_2 particles," *Ceram. Int.,* **36**[7] 2181-88 (2010).

[17]S. R. Skaggs, "A Brief History of Ceramic Armor Development," pp. 337-49. in 27th Annual Cocoa Beach Conference on Advanced Ceramics and Composites: A: Ceramic Engineering and Science Proceedings**.** John Wiley & Sons, Inc., 2008.

[18]B. Matchen, "Applications of Ceramics in Armor Products," *Key Eng. Mater.,* **122-124** 333-44 (1996).

[19]V. S. Galvez and L. S. Paradela, "Analysis of Failure of add-on armour for vehicle protection against ballistic impact," *Engineering Failure Analysis,* **16** 1837-45 (2009).

[20]G. E. Hauver, "The Ballistic Performance of Ceramic Targets,″ pp. 23-34 in Army Symposium of Solid Mechanics. (1993).

[21]V. Skorokhod and V. D. Krstic, "High strength-high toughness B_4C-TiB_2 composites," *J. Mater. Sci. Lett.,* **19**[3] 237-39 (2000).

[22]P. Lundberg and B. Lundberg, "Transition between interface defeat and penetration for tungsten projectiles and four silicon carbide materials," *Int. J. Impact Eng.,* **31**[7] 781-92 (2005).

[23]P. G. Karandikar, G. Evans, S. Wong, and M. K. Aghajanian, "Effects of Grain Size, Shape and Second Phases on Properties of Sintered SiC,″ in International Conference on Advanced Ceramics and Composites. **Vol. 30**, *Advances in Ceramic Armor V* Edited by J. J. Swab. (2009).

[24]R. W. Davidge and T. J. Green, "The strength of two-phase ceramic/glass materials," *J. Mater. Sci.,* **3**[6] 629-34 (1968).

[25]R. W. Rice, S. W. Freiman, and J. J. Mecholsky, "The Dependence of Strength-Controlling Fracture Energy on the Flaw-Size to Grain-Size Ratio," *J. Am. Ceram. Soc.*, **63**[3-4] 129-36 (1980).

[26]A. Krell, "A new look at grain size and load effects in the hardness of ceramics," *Mater. Sci. Eng., A* 277-84 (1998).

[27]A. Krell, "A new look at the influences of load, grain size and grain boundaries on the room temperature hardness of ceramics," *International Journal of Refractory Metals and Hard Materials*, **16** 331-35 (1998).

[28]X. F. Zhang, Q. Yang, and L. C. D. Jonghe, "Microstructure development in hot-pressed silicon carbide: effects of aluminum, boron, and carbon additives," *Acta Mater.*, **51** 3849-60 (2003).

[29]J. B. Wachtman, W. R. Cannon, and M. J. Matthewson, "Mechanical Properties of Ceramics," 2nd ed. John Wiley & Sons, Inc.: Hoboken, NJ, (2009).

[30]M. Übeyli, R. O. Yıldırım, and B. Ögel, "On the comparison of the ballistic performance of steel and laminated composite armors," *Materials & Design*, **28**[4] 1257-62 (2007).

[31]C. Hays and E. G. Kendall, "An analysis of Knoop microhardness," *Metallography*, **6**[4] 275-82 (1973).

[32]T. R. Simes, S. G. Mellor, and D. A. Hills, "A Note on the Influence of Residual Stress on Measured Hardness," *The Journal of Strain Analysis for Engineering Design*, **19**[2] 135-37 (1984).

[33]S. S. Chiang, D. B. Marshall, and A. G. Evans, "The response of solids to elastic/plastic indentation. I. Stresses and residual stresses," *J. Appl. Phys.*, **53**[1] 298-311 (1982).

[34]ASTM International, "Standard Test Method for Knoop Indentation Hardness of Advanced Ceramics", ASTM Standard C 1326-08E1, West Conshohocken, PA., (2008).

[35]T. L. Anderson, "Fracture Mechanics," 3rd ed. Taylor & Francis Group, LLC: Boca Raton, Fl, (2005).

[36]W. H. Gu and K. T. Faber, "Tensile Behavior of Microcracking SiC-TiB_2 Composites," *J. Am. Ceram. Soc.*, **78**[6] 1507-12 (1995).

[37]ASTM (ASTM International), "Dynamic Young's Modulus, Shear Modulus, and Poisson's Ratio for Advanced Ceramics by Impulse Excitation of Vibration", ASTM Standard C1259-08E1, West Conshohocken, PA., (2008).

[38]C. Kittel, "Introduction to Solid State Physics," 8th ed. John Wiley & Sons, Inc.: Hoboken, NJ, (2005).

[39]A. A. Griffith, "The Phenomena of Rupture and Flow in Solids," *Philos. Trans. R. Soc. London, A,* **221** 163-98 (1920).

[40]K. Li and T. Warren Liao, "Surface/subsurface damage and the fracture strength of ground ceramics," *Journal of Materials Processing Technology,* **57**[3–4] 207-20 (1996).

[41]ASTM International (ASTM), "Standard Test Method for Flexural Strength of Advanced Ceramics at Ambient Temperature", ASTM Standard C1161-02c, West Conshohocken, PA., (2008).

[42]G. R. Irwin, "Onset of Fast Crack Propagation in High Strength Steel and Aluminum Alloys," pp. 289-305 in Sagamore Research Conference Proceedings. **Vol. 2**. (1956).

[43]G. R. Irwin, "Analysis of Stresses and Strains Near the End of a Crack Traversing a Plate," *J. App. Mech.,* **24** 361-64 (1957).

[44]A. G. Evans, "Perspective on the Development of High-Toughness Ceramics," *J. Am. Ceram. Soc.,* **73**[2] 187-206 (1990).

[45]D. Munz, R. T. Bubsey, and J. L. J. Shannon, "Fracture Toughness Determination of Al_2O_3 Using Four-Point-Bend Specimens with Straight-Through and Chevron Notches," *J. Am. Ceram. Soc.,* **63**[5-6] 300-05 (1980).

[46]R. F. Cook and B. R. Lawn, "A Modified Indentation Toughness Technique," *J. Am. Ceram. Soc.,* **66**[11] c200-c01 (1983).

[47]G. R. Anstis, P. Chantikul, B. R. Lawn, and D. B. Marshall, "A Critical Evaluation of Indentation Techniques for Measuring Fracture Toughness: I, Direct Crack Measurements," *J. Am. Ceram. Soc.,* **64**[9] 533-38 (1981).

[48]W. Weibull, "A Statistical Theory of the Strength of Materials." in**.** Royal Technical University, Stockholm, 1939.

[49]W. Weibull, "A Statistical Distribution Function of Wide Applicability," *J. App. Mech.,* **18** 293-97 (1951).

[50]J. Gong, W. Si, and Z. Guan, "Weibull modulus of fracture strength of toughened ceramics subjected to small-scale contacts," *J. Mater. Sci.,* **36**[10] 2391-96 (2001).

[51]J. J. Swab, "Recommendations for Determining the Hardness of Armor Ceramics," *Int. J. Appl. Ceram. Technol.,* **1**[3] 219-25 (2004).

[52]R. W. Rice, C. C. Wu, and F. Boichelt, "Hardness–Grain-Size Relations in Ceramics," *J. Am. Ceram. Soc.,* **77**[10] 2539-53 (1994).

[53]T. S. Srivatsan, G. Guruprasad, D. Black, R. Radhakrishnan, and T. S. Sudarshan, "Influence of TiB_2 content on microstructure and hardness of TiB_2–B_4C composite," *Powder Technol.,* **159**[3] 161-67 (2005).

[54]L. Wang, H. Bei, Y. F. Gao, Z. P. Lu, and T. G. Nieh, "Effect of residual stresses on the hardness of bulk metallic glasses," *Acta Mater.,* **59**[7] 2858-64 (2011).

[55]M. A. Janney, "Mechanical Properties and Oxidation Behavior of Hot-Pressed SiC-15vol%-TiB_2 Composite," *Bull. Am. Ceram. Soc.,* **66**[2] 322-24 (1987).

[56]C. H. McMurtry, W. D. G. Boecker, S. G. Seshadri, J. S. Zanghi, and J. E. Garnier, "Microstrutcture and Material Properties of SiC-TiB_2 Composites," *Bull. Am. Ceram. Soc.,* **66**[21] 325-29 (1987).

[57]M.-J. Pan, P. A. Hoffman, D. J. Green, and J. R. Hellmann, "Elastic Properties and Microcracking Behavior of Particulate Titanium Diboride-Silicon Carbide Composites," *J. Am. Ceram. Soc.,* **80**[3] 692-98 (1997).

[58]J. D. Yoon and S. G. Kang, "Strengthing and toughening behaviour of SiC with additions of TiB_2," *J. Mater. Sci. Lett.,* **14** 1065-67 (1995).

[59]S. Baik and P. F. Becher, "Effect of Oxygen Contamination on Densification of TiB_2," *J. Am. Ceram. Soc.,* **70**[8] 527-30 (1987).

[60]K.-S. Cho, H.-J. Choi, J.-G. Lee, and Y.-W. Kim, "In situ enhancement of toughness of SiC-TiB_2 composites," *J. Mater. Sci.,* **33**[1] 211-14 (1998).

[61]C. Blanc and F. Thevenot, "Procesing of Ultra-Fine Dispersion of TiB_2 in SiC Ceramic Matrix," *Mater. Sci. Forum,* **235-238** 249-54 (1997).

[62]Y. Ohya, M. J. Hoffmann, and G. Petzow, "Sintering of in-Situ Synthesized SiC-TiB_2 Composites with Improved Fracture Toughness," *J. Am. Ceram. Soc.,* **75**[9] 2479-85 (1992).

[63]S. Prochazka, "Sintering of Silicon Carbide,″ pp. 239-52 in Second Army Materials Technology Conference. (1973).

[64]S. Prochazka and R. M. Scanlan, "Effect of Boron and Carbon on Sintering of SiC," *J. Am. Ceram. Soc.,* **58**[1-2] 72-72 (1975).

[65]G. B. Raju and B. Basu, "Densification, Sintering Reactions, and Properties of Titanium Diboride With Titanium Disilicide as a Sintering Aid," *J. Am. Ceram. Soc.*, **90**[11] 3415-23 (2007).

[66]R. Goodall, J. F. Despois, and A. Mortensen, "Sintering of NaCl powder: Mechanisms and first stage kinetics," *J. Eur. Ceram. Soc.*, **26**[16] 3487-97 (2006).

[67]M. N. Rahaman, "Ceramic Processing.″ Taylor & Francis Group, LLC: Boca Raton, FL, (2007).

[68]R. A. Alliegro, L. B. Coffin, and J. R. Tinklepaugh, "Pressure-Sintered Silicon Carbide," *J. Am. Ceram. Soc.*, **39**[11] (1956).

[69]J. S. Reed., "Principles of Ceramic Engineering,″ Second ed. John Wiley & Sons, Inc.: New York, NY, (1994).

[70]J. M.W. Chase, C. A. Davies, J. J.R. Downey, D. J. Frurip, R. A. McDonald, and A. N. Syverud, "NIST-JANAF Thermochemical Tables," http://kinetics.nist.gov/janaf/.

[71]J. J. Cao, W. J. MoberlyChan, L. C. De Jonghe, C. J. Gilbert, and R. O. Ritchie, "In Situ Toughened Silicon Carbide with Al-B-C Additions," *J. Am. Ceram. Soc.*, **79**[2] 461-69 (1996).

[72]H. Endo, M. Ueki, and H. Kubo, "Hot pressing of SiC-TiC composites," *J. Mater. Sci.*, **25**[5] 2503-06 (1990).

[73]X. F. Zhang, M. E. Sixta, and L. C. D. Jonghe, "Grain Boundary Evolution in Hot-Pressed ABC-SiC," *J. Am. Ceram. Soc.*, **83**[11] 2813-20 (2000).

[74]M. Miura, T. Yogo, and S. I. Hirano, "Phase separation and toughening of SiC-AIN solid-solution ceramics," *J. Mater. Sci.*, **28**[14] 3859-65 (1993).

[75]D. Ray, M. Flinders, A. Anderson, R. A. Cutler, and W. Rafaniello, "Effect of Room-Temperature Hardness and Toughness on the Ballistic Performance of SiC-Based Ceramics,″ in International Conference on Advanced Ceramics and Composites. **Vol. 26**, *Advances in Ceramic Armor* Edited by J. J. Swab.

[76]S. J. Park, K. Cowan, J. L. Johnson, and R. M. German, "Grain size measurement methods and models for nanograined WC–Co," *International Journal of Refractory Metals and Hard Materials*, **26**[3] 152-63 (2008).

[77]M. Taya, S. Hayashi, A. S. Kobayashi, and H. S. Yoon, "Toughening of a Particulate-Reinforced Ceramic-Matrix Composite by Thermal Residual Stress," *J. Am. Ceram. Soc.*, **73**[5] 1382-91 (1990).

[78]D.-H. Kuo and W. M. Kriven, "Mechanical behavior and microstructure of SiC and SiC/TiB_2 ceramics," *J. Eur. Ceram. Soc.*, **18**[1] 51-57 (1998).

[79]Z. Li and R. C. Bradt, "Thermal Expansion and Thermal Expansion Anisotropy of SiC Polytypes," *J. Am. Ceram. Soc.*, **70**[7] 445-48 (1987).

[80]M. K. Ferber, P. F. Becher, and C. B. Finch, "Effect of Microstructure on the Properties of TiB_2 Ceramics," *J. Am. Ceram. Soc.*, **66**[1] C-2-C-3 (1983).

[81]H. Cai, W. H. Gu, and K. T. Faber, "Microcrack Toughening in a SiC-TiB_2 Composite," in Proceedings of the American Society for Composites Fifth Technical Conference; composite materials in transition.

[82]W. H. Gu, K. T. Faber, and R. W. Steinbrech, "Microcracking and R-curve behavior in SiC-TiB_2 composites," *Acta Metall. Mater.*, **40**[11] 3121-28 (1992).

[83]D. Bucevac, B. Matovic, B. Babic, and V. Krstic, "Effect of post-sintering heat treatment on mechanical properties and microstructure of SiC–TiB_2 composites," *Mater. Sci. Eng., A*, **528**[4–5] 2034-41 (2011).

[84]S. S. Ordan'yan, A. I. Dmitriev, E. K. Stepanenko, N. Y. Aulova, and N. E. Semenov, "SiC-TiB_2 system - A base of high-hardness wear-resistant materials," *Powder Metallurgy and Metal Ceramics*, **26**[5] 375-77 (1987).

[85]B.-W. Lin, M. Imai, T. Yano, and T. Iseki, "Hot-Pressing of β-SiC Powder with Al-B-C Additives," *J. Am. Ceram. Soc.*, **69**[4] C-67-C-68 (1986).

[86]S.-H. Lee, "Low Temperature Pressureless Sintering of SiC Using an Aluminum Borocarbide Additive," *J. Am. Ceram. Soc.*, **94**[9] 2746-48 (2011).

[87]W. A. Chupka, J. Berkowitz, C. F. Giese, and M. G. Inghram, "Thermodynamic Studies of Some Gaseous Metallic Carbides," *The Journal of Physical Chemistry*, **62**[5] 611-14 (1958).

VITA

Derek Scott King was born on May 5th, 1988 in Kansas City, MO. In August of 2006 Derek started his undergraduate degree as an aerospace engineer at the University of Missouri-Rolla (now Missouri University of Science and Technology). Derek later decided to join the Ceramic Engineering Department. During his undergraduate career, Derek joined the student groups Material Advantage and Keramos and was a founding member of the Gaffers Guild. Derek also spent time at a REU, co-op, and was an undergraduate research assistant at Missouri S&T. Knowing he wanted to continue research, Derek spent his last semester taking undergraduate and graduate courses at Missouri S&T. Derek received his B.S. degree in Ceramic Engineering from Missouri S&T in December, 2010.

Derek began his graduate work as a Masters student in January of 2011 working on advanced ceramics for armor applications. During his first semester as a graduate student, Derek was awarded a Chancellors Fellowship from the recommendation of his advisors Bill Fahrenholtz and Greg Hilmas. During his time as a Masters student, Derek assisted with the Mechanical Properties of Ceramics lab. Derek received his M.S. degree in Ceramic Engineering from Missouri S&T in December, 2012. After enjoying teaching with the lab and conducting research, Derek plans to stay at Missouri S&T where he will work toward a Ph.D. in Ceramic Engineering.